

Biologically effective daily radiant exposure for erythema appearance, previtamin D₃ synthesis and clearing of psoriatic lesions derived from erythema broadband meters at Belsk, Poland, for the period 1976-2023

Janusz W. Krzyścin¹, Agnieszka Czerwińska¹, Bonawentura Rajewska-Więch¹, Janusz Jarosławski¹, Piotr S. Sobolewski¹, Izabela Pawlak¹

¹ Institute of Geophysics, Polish Academy of Sciences, Warsaw, 01-452, Poland

Correspondence to: Janusz W. Krzyścin (jkrzys@igf.edu.pl)

Abstract. A long-term series of exposures to solar ultraviolet radiation (UVR) is required to assess the risks and benefits of radiation on different human biological processes. However, homogenisation of the amount of biologically effective solar energy (i.e. energy weighted according to the sensitivity of the selected biological process to solar radiation) reaching the Earth's surface over long periods is challenging due to changes in measurement methods and instruments. This paper presents the world's longest homogenised time series of biologically effective daily radiant exposures (DRE) from regular monitoring with different erythema broadband radiometers (EBRs) operated at the Central Geophysical Laboratory of the Institute of Geophysics, Polish Academy of Sciences (IG PAS), Belsk (20.79°E, 51.84°N) from 1 January 1976 to 31 December 2023. The following biological effects were considered: ~~the~~ erythema, cutaneous synthesis of previtamin D₃, and clearing of psoriatic lesions. The data for the latter two biological effects are estimated based on the proposed method of using EBR measurements to calculate other non-erythema DRE. The following EBRs were used in the monitoring: Robertson-Berger ~~meter~~ (1975–1992), Solar Light model 501 (1993–1994 with #927, 1995–2013 with #2011) and Kipp-~~&~~Zonen UV-AE-T #30616 from 5 August 2013 to the present. From 1976 to 2013, the homogenisation procedure consisted of comparing the measured erythema DRE and daily maximum of UV index (UVI_{MAX}) with the corresponding ~~synthetic modelled~~ values from simulations using a radiation transfer model for cloudless conditions. Between 2014 and 2023, the EBR data were compared with data from a collocated reference instrument, the Brewer Mark II #64 ~~spectrometer-spectrophotometer~~. Such comparisons resulted in a set of multipliers that were applied to the EBR measurements. Two different versions of the homogenisation method were applied analysing modelled and observed values for erythema DRE and UVI_{MAX} assuming different criteria for cloudless days. Three regression models of the erythema data on common UVR ~~indices proxy data~~ (total column ozone, aerosol optical depth and global clear sky irradiance index) were used to reconstruct the UVR data from the beginning of the Belsk observations, allowing further validation of the homogenised UVR data. Linear trends calculated showed a statistically significant increase in erythema annual and summer (June to August) radiant exposures of about 6 % per decade over the period 1976–2005. Thereafter, no trend was observed. ~~The same~~ Similar trend estimates were found for all biological effects considered. The data are made freely available via the following repository: <https://doi.org/10.1594/PANGAEA.972139> (Krzyścin et al., 2024). An additional version of the re-evaluated data, together with the corresponding clear sky and proxy data used in the UVR data reconstruction, is archived at:

https://doi.org/10.25171/InstGeoph_PAS_IGData_Biologically_Effective_Solar_Radiation_Belsk_1976_2023
(Krzyścin, 2024).

Keyword(s): erythral broadband radiometer; biologically effective irradiance, homogenisation, radiant exposure

1 Introduction

Molina and Rowland (1974), winners of the 1995 Nobel Prize in Chemistry, argued that man-made chlorofluorocarbons (CFCs), which were widely used in industry in the 1970s, could reach the stratospheric ozone layer where they would be destroyed by short-wave ultraviolet radiation (UVR), releasing free chlorine atoms and causing stratospheric O₃ depletion in the catalytic reaction cycle. Solar radiation in the shortest part of its spectrum that reaches the Earth's surface (290–315 nm), known as UV-B, is strongly absorbed by stratospheric ozone. The discovery of the ozone hole over Antarctica (Chubachi, 1984; Farman et al., 1985) and the predicted decreasing trend in total column ozone (TCO₃) in other regions have stimulated interest in establishing continuous monitoring of UV-B irradiance reaching the ground. In addition, there is growing evidence that such UVR trends can cause various adverse health effects, such as skin cancers (including the deadly melanoma), DNA damage, immunosuppression, oxidative stress and skin ageing (Neale et al., 2023).

Solar UV-B radiation from space is attenuated as it passes through the atmosphere due to light scattering (by cloud particles, atmospheric gases and aerosols) and absorption (by O₃, NO₂, SO₂ and aerosols). The attenuation of light increases with its path length through the atmosphere (i.e. usually described by the air mass), so solar elevation and ground surface altitude are key parameters to consider in surface UVR modelling. Other factors forcing UVR variability at the surface that are often used as proxies for atmospheric UV-B attenuation are total column O₃ (TCO₃) to account for UVR absorption by ozone, the clear sky index (CI) (i.e. a quotient of the all-sky global solar irradiance (G) at the surface and the corresponding synthetic modelled clear-sky value (G₀) to account for combined cloud/aerosol scattering effects on UVR), and aerosol optical depth (AOD) in the solar UV range (parameterising UVR attenuation by aerosols). TCO₃ and G have been found to be the most effective important factors for modelling surface UV-B radiation (Koepeke et al., 2006; den Outer et al., 2010).

In the early 1970s, the broadband Robertson-Berger (RB) meter was developed to measure the biologically effective (BE) UVR that causes skin redness, also known as erythema (Berger, 1976). The spectral characteristics of RB resembled the erythral sensitivity of human skin. RB instruments began continuous monitoring of erythral irradiance in 1974 at eight sites in the United States (Scotto et al., 1988). During the 1970s, instruments were operated in other countries (Austria, Australia, Germany, Poland, Sweden, Switzerland) (WMO, 1977). At the beginning of this global network, RB meters were calibrated using a travelling standard meter provided by the Photobiology Center at Philadelphia University. After a few years, at some stations, including the Institute of Geophysics, Polish Academy of Sciences (IG PAS) station at Belsk (51.84°N, 20.78°E), this calibration method was replaced by comparisons with values modelled by the radiative transfer model. The Dave-Halpern model (Dave and Halpern, 1976) was used to estimate erythemally weighted irradiance for cloudless sky conditions to calibrate the Belsk data (Słomka and Słomka, 1985). Serious drawbacks of RB measurements were that their results were reported in relative units (counts), temperature sensitivity, a lot of manual work in data preparation, sometimes rapid ageing, and difficulties in accurately converting counts into the so-called sunburn unit (the minimum erythral radiation exposure that causes redness of the skin). These problems were significantly reduced in a new version of the RB meter, a prototype of the current erythral broadband radiometer (EBR), developed in

the late 1980s as a result of collaboration between IG PAS and the Institute of Medical Physics of the University of Innsbruck (Blumthaler et al., 1989; Słomka and Słomka, 1993). Further prototype work at Solar Light (SL) Co. in Philadelphia resulted in the production of a commercial SL Biometer Model 501A, which replaced the RB meter.

Other EBR versions were introduced in the 1990s, including those from Yankee Environmental Systems (Turner Falls, USA) and Kipp-~~and~~ & Zonen (KZ) Co. (Delf, Netherlands). However, there was a need to standardise the correction procedure for the broadband UVR meters as it became apparent that the calibration provided by the manufacturer could not be relied upon even for the same type of instrument (Leszczynski et al., 1998). A standard calibration method that takes into account the individual spectral characteristics of the instrument and the loss of sensitivity has been proposed (Hülsen and Gröbner 2007). However, uncertainties of ~7 % can still be expected for well-maintained EBRs (Gröbner et al., 2009).

Long-term series of surface UVR from ground-based observations with a length of at least a few decades are rare. To the authors' knowledge, the longest UVR monitoring series began in Moscow in 1968 with a broadband (300–380 nm) instrument developed at the Moscow State University Meteorological Observatory (Chubarova et al., 2000). One of the world's longest measurements of solar UVR at the Earth's surface (and probably the longest taken by erythral broadband instruments) are from Belsk. Measurements began in 1975 and continuous monitoring started on 1 January 1976. From a global perspective, the first UVR results appeared at the World Ozone and Radiation Data Centre (WOUDC) in 1989, but continuous UVR time series over three decades are only available for a limited number of stations including: Uccle (Belgium), Edmonton, Resolute, Toronto, Churchill, Saturna Island (Canada), Tateno (Japan) and Syowa (Antarctica) (WOUDC, 2025). ~~Database~~The data archive of Network for the Detection of Atmospheric Composition Change (NDACC) also include ~~also~~ stations with at least of three decades of UVR measurements such as Lauder (New Zealand), Mauna Loa (USA) and three Antarctica stations – Arrival Heights, Palmer Station and South-Pole (NDACC, 2025).

This article presents a retrospective evaluation of all UVR measurements (1976–2023) at Belsk made with different EBRs including: RB (1976–1992), SL Biometer model ~~501-A~~ (SL501-A, 501A, SL501A) (two instruments were used #927 and #2011 for the period 1993–1994 and 1995–2013, respectively) and KZ UV-AE-T #30616 (KZ616) from 5 August 2013 to the present. The re-evaluation for the period 1976–2013 is based on a comparison of the measurements with the ~~synthetic~~modelled daily erythral radiant exposure and the UV index at local solar noon from a radiative model simulation for clear sky conditions using TCO₃ and AOD measured at Belsk as model input parameters. The quality of the KZ616 data (2013–2023) will be accessed through comparisons with clear-sky erythral irradiances simultaneously measured by the well-maintained Brewer spectrophotometer Mark II #64 (BS64). The details of the Brewer maintenance can be found in Czerwińska and Krzyścin (2024a). Erythral daily radiant exposures (DRE) for the entire period of the UVR measurements at Belsk will be transferred to the corresponding vitamin D₃ and antipsoriatic DRE using a method proposed by Czerwińska and Krzyścin (2024a). A comparison of these DRE with those from BS64 spectral measurements in the period 2014–2023 will indicate the accuracy of the proposed reconstruction method of past BE data based on a statistical approach using typical proxies (TCO₃ and G) characterising atmospheric UVR attenuation. Finally, trend calculations ~~in~~for annual (January–December) and summer (June–August) radiant exposures (RE) for all biological effects considered and three versions of ~~the~~ recalculated UVR data from 1976–2023 will be presented to confirm the robustness of the long-term changes in the BE radiation measured at Belsk.

2 Materials and Method

2.1 UVR monitoring

Recording of erythema irradiance with a standard RB meter (detector recorder No. 40) started in May 1975 at Belsk, but continuous monitoring began on 1 January 1976 and lasted until 1994. From May 1993, in parallel with the RB measurements, the monitoring of erythema irradiance using the SL Biometer ~~501-A501A~~ #927 was initiated in order to establish monthly transfer coefficients for converting the RB output in sunburn units (SU) into erythema units, i.e. the minimum erythema dose (MED) causing skin redness in typical Caucasian skin, which was entered into the SL Biometer ~~501-A501A~~ measurements (Puchalski, 1995). ~~It was assumed that 1 MED = MEDs were converted to the erythema doses by multiplication with~~ $210 J_{\text{eryt}} m^{-2}$, where J_{eryt} denotes spectral irradiance integrated over time and wavelengths (290–400 nm) after weighting by the erythema action spectrum. Simultaneous measurements continued until December 1994, and all erythema DRE measured with the RB meter before 1993 were multiplied by these transfer coefficients to ~~obtain~~produce data comparable to those obtained with the SL Biometer ~~501-A501A~~.

As the RB meter showed sensitivity to ambient temperature, a correction for temperature effect was applied to the raw daily RB values (Borkowski, 1998) using empirical formulas proposed by Koskela et al. (1994). In addition, the RB Belsk series was also found to be affected by a change in calibration method in 1985, as the Dave-Halpern model (Dave and Halpern, 1976) calculations for cloudless conditions replaced field comparisons with the travelling standard instrument. This resulted in a downward step change of 14 % in the UVR series (Borkowski, 2000). The re-evaluated time series of erythema DRE for the period 1976–1992 as made by Borkowski (2008) was archived and formed part of the Belsk’s erythema time series (1976–2023), which is further homogenised in this study.

Subsequent UVR measurements included ~~SL501-ASL501A~~ # 927 (1993–1994) and #2011 (1995–2013), which were ~~only roughly~~ calibrated by the instrument manufacturer prior to shipment, ~~but these calibrations proved to be very inaccurate~~ Therefore, this paper is another attempt to recalculate past UVR data. In 2005, KZ616 was added to the IG PAS UV network and served as the reference instrument. It was not used for everyday UVR monitoring but only for occasional international calibration campaigns to provide a source for further calibrations with our SL biometers operating in Belsk and Hornsund (Spitzbergen). KZ616 started regular UVR monitoring on 5 August 2013, replacing the raw ~~SL501-ASL501A~~ #2011, as BS64 (normally measuring TCO_3 and Umkehr ozone at Belsk since 1992) was established as the new UVR reference instrument for the IG PAS network, which has been in operation until now. The performance of KZ616 has proven to be very stable and it is still ~~involved~~used in regular UVR monitoring.

In the following, we use the term “raw data” for the results of the EBR measurements in $W m^{-2}$ and $J m^{-2}$ that were previously archived in the internal databases of IG PAS before the release of the Krzyścin et al. (2024) and Krzyścin (2024) databases.

2.2 Ancillary data

Daily representatives of TCO_3 at Belsk are taken from the IG PAS data portal (Krzyścin, 2024), which contains results of daily average TCO_3 measurements ~~throughout the day~~, prepared for UVR modelling purposes. For example, the most reliable daily representative value of TCO_3 (marked with flag no. 1) was calculated as an average of the most accurate measurements (the so-called direct sun measurements) made by the Dobson

spectrophotometer between 9:00 and 13:00 UTC. The least accurate case of ground-based TCO_3 observations (with flag no. 5) occurred under cloudy and low sun elevation conditions, i.e. before 9:00 and after 13:00 UTC. In this case, only the least reliable Dobson observations were available for calculating the daily TCO_3 representative under overcast zenith and high air masses. In the rare cases when ground observations were not available, satellite data (flag 6 or 7 depending on the data source) and/or TCO_3 reanalysis data (flag 8) were used.

The daily representative of CI, DCI, which is further used in regression models (Sect. 2.3.4), is calculated as the quotient of the daily integrals (sunrise to sunset) of G and G_0 . Typically, the former values were obtained from routine monitoring of global solar irradiance by various pyranometers (since 1965) including the following instruments: Kipp & Zonen CM 6, Sonntag PRM-2, Kipp & Zonen CM 5, Kipp & Zonen CM 11, and Kipp & Zonen CM 21. The data were calibrated using the Polish national standard, which had previously been adjusted to the world standard during inter-comparison campaigns at the World Radiation Centre in Davos, Switzerland. In addition, the Campbell-Stokes sunshine recorder provided the duration of sunshine per day to pre-select sunny days. All these data are archived in the IG PAS Data Portal (Krzyścin, 2024).

To validate the corrected UV observations at Belsk, the long-term variability of BE radiation was also obtained from the UVR reconstruction models (Section 2.3) using proxies (TCO_3 and DCI) from the ground-based observations and reanalysis datasets. The European Centre for Medium-Range Weather Forecasts (ECMWF) v5 (ERA5) reanalysis provides, in addition to many other variables, intra-day TCO_3 values, G_0 , and G for the period 1940–2024, which are freely available on the ERA5 (2025) website. Also included are data (from 1 January 1980 to the present) downloaded from the Modern-Era Retrospective Analysis for Research and Applications version 2 (MERRA-2) database (GMAO, 2025) using the Giovanni data search tool, which is freely available on the Giovanni (2025) website.

Table 1. The Belsk's instruments and their working periods.

Data	Instrument/data	Operation period	Reference
Daily ERE and UV Index	Robertson–Berger Meter	1976–1994	Krzyścin et al. (2024)
	SL Biometer 501 A # 927	1992–1994	
	SL Biometer 501 A # 2011	1995–2013	
	Kipp-Zonen UV-AE-T # 30616	2013–present	
TCO_3	Dobson Spectrophotometer # 84	1963–present	Krzyścin (2024)
	Ozone Monitoring Instrument (OMI)	2004–present	ESRL (2025)
	Ozone Mapping and Profiling Suite (OMPS) Nadir-Mapper (NM) instrument	2012–present	ESRL (2025)
SunDur	Campbell–Stokes sunshine recorder	1966–1968, 1970–1973, 1975–present	Krzyścin (2024)
G	Kipp CM 6	1965–1980	Krzyścin (2024)
	Sonntag PRM-2	1981–1987	
	Kipp&Zonen CM 5	1988–1991	
	Kipp&Zonen CM 11	1992–2010	
	Kipp&Zonen CM 21	2010–present	
$\text{AOD}_{340\text{nm}}$	Sonntag pyrheliometers	1976–2013	Krzyścin (2024)
	CIMEL CE 318-T	2004–present	
G and G_0	ERA5 reanalysis	1940–present	ERA5 (2025)
G_0	MERRA-2 reanalysis	1980–present	GMAO (2025)

Atmospheric aerosols can be significant drivers of surface UVR, especially under clear sky conditions (Krzyścin and Puchalski, 1998). The column properties of aerosols can be obtained from ground-based observations and used in the modelling of radiative transfer in the atmosphere. Aerosol properties are described by various characteristics (e.g. including AOD, single scattering albedo, asymmetry factor). In this article, we use Belsk's AOD at 340 nm (IG PAS Data Portal, Krzyścin (2024)), which is estimated from the Linke turbidity factor measurements with Sonntag pyrhelimeters between 1976 and 2013 (Posyniak et al., 2016) and from the co-located solar photometer CIMEL CE 318-T (2004–2023) operating within the Aerosol Robotic Network (AERONET) (AERONET, 2025). Other aerosol properties are kept constant and equal to their typical values for the rural site. Taking into account climatology of the Belsk's aerosol characteristics (AERONET, 2025) values of 0.95 and 0.69 are taken for single scattering albedo and asymmetry factor, respectively. Table 1 summarises the sources of the data used in this paper.

2.3 UVR models

2.3.1 Clear-sky model

Radiative transfer model simulations for clear sky conditions are used to quantify and correct biases in the output of the Belsk UVR radiometers. To speed up the calculations, ~~the~~ look-up tables were obtained using the Tropospheric Ultraviolet and Visible (TUV) Radiative Transfer Model (TUV, 2025). The TUV model, which was introduced by Madronich (1993), has since been widely used in UVR simulations. ~~Synthetic~~ Modelled clear-sky values of BE (erythema, previtamin D₃ synthesis, clearing of psoriasis lesions) RE in day D , $RE_{EFF,CS}(D)$ in $J_{EFF} m^{-2}$, and irradiance at ~~noon, $Ir_{EFF,CS}(t=noon)$, local solar noon, $Ir_{EFF,CS,MAX}$~~ in $W_{EFF} m^{-2}$, respectively, are calculated using the following formulas:

$$Ir_{EFF,CS}(t) = \int_{290\text{ nm}}^{400\text{ nm}} Ir_{CS}(\lambda, t) AS_{EFF}(\lambda) d\lambda \quad (1)$$

$$RE_{EFF,CS}(D) = \int_{Sunrise(D)}^{Sunset(D)} Ir_{EFF,CS}(t) dt \quad (2)$$

$$Ir_{EFF,CS}(t) = \int_{290\text{ nm}}^{400\text{ nm}} Ir_{CS}(\lambda, t) AS_{EFF}(\lambda) d\lambda \quad (2)$$

where $I_{r_{CS}}(\lambda, t)$ is the spectral irradiance at time t and at wavelength λ , and $AS_{EFF}(\lambda)$ denotes the action spectrum for specific biological effect EFF: EFF=ERYT for erythema (CIE 2019), EFF=VITD3 for photosynthesis of previtamin D₃ in human skin (CIE 2006), and EFF=PSOR for psoriasis clearing (Krzyścin et al., 2012). Figure 1 presents the action spectra used.

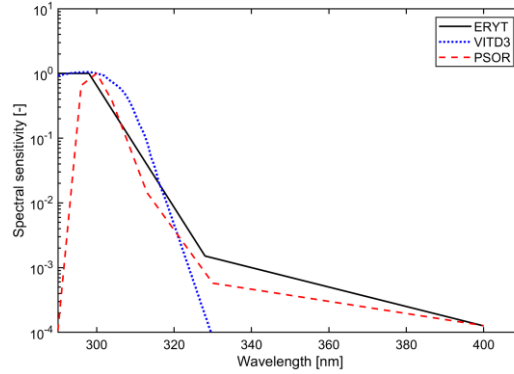
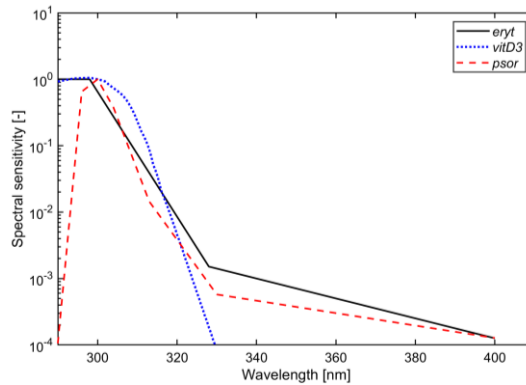


Figure 1. Normalised action spectra for the specific biological effects: erythema (ERYT), photosynthesis of previtamin D₃ in human skin (VITD3), psoriasis clearing (PSOR).

Input to the clear-sky version of TUV model (daily representatives of TCO₃, annual and monthly mean AOD at 340 nm for the period 1976–2013 and 2014–2023, respectively) and output ($RE_{EFF,CS}(D)$ and $I_{r_{EFF,CS}}(t=noon), I_{r_{EFF,CS,MAX}}$ where EFF={ERYT, VITD3, PSOR}), are archived in IG PAS Data Portal (Krzyścin, 2024).



2.3.2 Re-evaluation of the UVR measurements

Model simulations of erythema DRE and noon-UVI_{MAX} under cloudless sky provide a basis for the correction procedure of the past UVR data. A selection of clear-sky conditions throughout the entire day from the daily proxy values (relative sunshine duration and DCI), which were available for Belsk, is not straightforward as only the examination of the daily course of these measurements would allow to capture cloudless moments within the day. Thus, two different sets of correction coefficients are proposed, called CC1 and CC2.

The intraday UVR measurements at Belsk from 1976 to 2023 can be clearly divided into three periods: 1 January 1976–31 December 1992, 1 January 1993–4 August 2013, and 5 August 2013–31 December 2023, according to the different broadband instruments used for UVR monitoring, i.e. RB, SL501A, and KZ616, respectively. For the first period, only the erythema DRE were archived, whereas for other periods daily maximum of UV index (UVI_{MAX}) was also available (equal to the value of erythema irradiance at local solar noon during a

cloudless day). There were also periods when both instruments were operated simultaneously for calibration purposes: March 1992–December 1994 (RB versus ~~SL501~~ASL501A), 5 August 2013–31 December 2014 (~~SL501~~ASL501A #2011 versus KZ616), and 5 August 2013–31 December 2023 (KZ616 versus BS64).

The correction procedure before 5 August 2013 consisted of comparing the raw erythemal data with the corresponding ~~syntheti~~modelled values obtained from the radiative model simulations (described in Sections 2.3.1) for days when ancillary data indicated that the sky was clear throughout the day. The LOcally Weighted Scatterplot Smoothing (LOWESS) proposed by Cleveland (1979) was used to extract the smoothed pattern of the multipliers of the raw UVR data, i.e. the correction coefficients (CCs), from the daily ratios between ~~syntheti~~modelled and erythemal REs (for version CC1 of the correction) or from the ratios between UVI_{MAX} (version CC2). The following conditions were applied for the selection of clear sky data used in the two correction methods:

- CC1 – direct sun TCO₃ measurements occurred between 9:00–13:00 UTC (code 1 for the TCO₃ observation in IG PAS Data Portal, Krzyścin (2024)) and the daily difference between the observed and the theoretical maximum sunshine duration is less than 30 minutes at solar zenith angles (SZAs) ~~below~~less than 85°. This limit was chosen because broadband UVR measurements at larger SZAs are unreliable and the Campbell-Stokes instruments starts when direct sun irradiance exceeded 120 W m⁻².
- CC2 – for TCO₃, the same condition was set as for CC1, and the ratio between the observed and theoretical sunshine hours (for SZA < 85°) is not less than 85 %. CC2 values have only been calculated for the period since 1 January 1993. Prior to this date, a re-evaluation of the RB data with a model mimicking the KZ radiometer measurements by Krzyścin et al. (2011) showed that the correction was not necessary, i.e. CC2=1. This choice is also confirmed here by the constant long-term patterns of ~~CC1~~the ratio between modelled and observed DRE in the period 1976-1992 (Fig. 6a), and only a small jump in the differences between CC1 and CC2 in 1992/1993 (Fig. 6b)see Sect. 3.2.1 for more details).

~~Different criteria for the selection of cloudless days would result in even greater differences between the two CC versions. In addition, the~~The smoothing procedure was applied to the long (1976-2013) and short (1993-2013) UVR time series for the CC1 and CC2 versions, respectively. ~~We would like to have two different sets of correction coefficients to find out how the long term pattern of biologically effective radiation is sensitive to the corrections~~A small jump (~0.01) in the smoothed UVI_{max} ratio was found in January 1993 (Sect. 3.2.1), which further corroborates the selection of CC2 = 1 prior to 1993.

The CC1 and CC2 versions of the re-evaluated Belsk UVR data are stored in the following free-access data archives: <https://doi.org/10.1594/PANGAEA.972139> (Krzyścin et al., 2024) and https://doi.org/10.25171/InstGeoph_PAS_IGData_Biologically_Effective_Solar_Radiation_Belsk_1976_2023 (Krzyścin, 2024), respectively.

2.3.3 Reconstruction of BE radiation from the erythemal data

Broad-band instruments for measurement of the erythemal irradiance can also estimate non-erythemal irradiance by multiplying the erythemal irradiance by the so-called conversion factors (CF_{EFF}) derived from spectral UVR measurements and/or radiative transfer simulations (Schmalwieser et al., 2022; Czerwińska and Krzyścin, 2024a):

$$Ir_{EFF}(t) = CF_{EFF}(TCO_3, SZA) \times Ir_{ERYT}(t), \quad _ (3)$$

where SZA denotes the solar zenith angle at time t . Following this concept, the daily radiant exposure for previtamin D₃ synthesis and psoriasis clearance in year (YR), month (MM), and day of month (DD) $RE_{VITD3}(YR, MM, DD)(Y, M, D)$ and $RE_{PSOR}(YR, MM, DD)(Y, M, D)$, respectively, were estimated using the daily conversion factor, CF_{EFF}^* , applied to the erythral DRE ($RE_{ERYT}(YR, MM, DD)(Y, M, D)$):

$$RE_{EFF}(YR, MM, DD)(Y, M, D) = CF_{EFF}^*(TCO_3, JD)(TCO_3, DY) \times RE_{ERYT}(YR, MM, DD)(Y, M, D), \quad EFF = \{VITD3, PSOR\}, \quad (4)$$

where CF_{EFF}^* depends on TCO_3 and JD (Julian-DY (day number of the year corresponding to the current day $\{YR, MM, DD, Y, M, D\}$)). CF_{EFF}^* and CF_{EFF} values were obtained from radiative transfer model simulations. The time series (1976–2023) of the conversion factors, $RE_{EFF}(YR, MM, DD)(Y, M, D)$, and the corresponding noon value of the biologically effective irradiance at local solar noon, $I_{EFF}(t = \text{noon})$, $I_{EFF,MAX}$ have been archived in the IG PAS Data Portal (Krzyścin, 2024).

2.3.4 Regression models

The CCs described in section 2.3.2 were obtained for cloudless conditions and applied to all-sky conditions, where the contribution of the diffuse part of the radiation increases with cloud cover and dominates under overcast conditions. It cannot be ~~excluded~~ruled out that the instruments used to monitor UVR at Belsk have their own specific characteristics for recording diffuse radiation, and that CF_{EFF}^* and CF_{EFF} in Eqs. (3–4) ~~should~~ also depend on the combined characteristics of clouds and instruments. To test whether this is the case, we investigated how different regression models, which were trained using the UVR data collected between 2014 and 2023 (for this period, the quality of the broadband radiometer was confirmed by the Brewer Mark II observations), reproduce the daily doses of erythral radiation throughout the 1976–2023 monitoring period.

The first model (Mod1) is based on clear-sky spectra determined with the RT model discussed in Section 2.3.1 and a cloud modification factor (CMF) derived from DCI data. The second and third models (Mod2 and Mod3) are based on TCO_3 and DCI data evaluated on a monthly basis. TCO_3 and DCI were either taken from observations at Belsk (Mod2) or ERA5 reanalysis (Mod3).

According to a widely used UVR modelling concept (e.g. Rieder et al., 2008; den Outer et al., 2010; Čížková et al., 2018; Czerwińska and Krzyścin, 2024b) the erythral DRE on the current a given day $\{YR, MM, DD, Y, M, D\}$, $RE_{ERYT}(YR, MM, DD, Y, M, D)$, is the product of CMF (empirical function of DCI parameterising UVR attenuation by clouds) for that day, and the ~~synthetic modelled~~ clear-sky value $RE_{ERYT,CS}$ (Section. 2.3.1):

$$RE_{ERYT}(YR, MM, DD)(Y, M, D) = CMF(DCI(YR, MM, DD))(DCI(Y, M, D)) \times RE_{ERYT,CS}(YR, MM, DD), \quad (5)$$

CMF is calculated here as a power function with the regression coefficients, α and β , depending on SZA at local solar noon, SZA_N , for the ~~current~~ day $\{YR, MM, DD, Y, M, D\}$:

$$CMF(DCI(YR, MM, DD))(DCI(Y, M, D)) = \alpha[DCI(YR, MM, DD)]^\beta \alpha[DCI(Y, M, D)]^\beta, \quad (6)$$

where estimates for the regression coefficients, α and β , were obtained from the 2014–2023 data when the KZ616 measurements were well matched to the BS64 data (Section Sect. 3.1). In DCI ($DCI = DG \cdot DG_0^{-1}$) calculation, the

daily integral of global solar irradiance, DG , is from observations at Belsk or ERA5, and its clear-sky equivalent, DG_0 , from ERA5 (before 1980), and thereafter the mean of ERA5 and MERRA-2 values.

The standard least-squares subroutine (Matlab function – $fitlm(x,y)$) provided the estimates for three arbitrarily selected $SZA_{local\ solar\ noon} (SZA_N)$ ranges (Table 2). These regression coefficients were used for the reconstruction of the RE_{ERYT} time series for the entire period of UVR measurements (1 January 1976 up to 31 December 2023). This model will be referred to as Mod1 in ~~the following text~~ this paper.

Table 2. Estimates of the regression coefficients, α and β , describing the attenuation of erythral DRE by the empirical model, -Mod 1, defined by Eqs. (5–6), for the three SZA ranges ~~at~~ of local solar noon (SZA_N).

Regression Coefficients					
α	β	α	β	α	β
$SZA_N < 45^\circ$		$SZA_N \geq 45^\circ$ and $< 60^\circ$		$SZA_N \geq 60^\circ$	
0.954	0.844	0.918	0.750	0.960	0.697

The next two regression models were trained using the monthly averages of erythral DRE, $RE_{ERYT}(YR, MM)(Y, M)$, for month MMM in year YRY (from 2014 up to 2023) averaging all available daily $RE_{ERYT}(YR, MM, DD)(Y, M, D)$ values in MMM month for YRY year. The corresponding long-term (2014–2023) monthly means, $RE_{ERYT}^*(MM)(M)$, is from the averages of all data for this calendar month. The idea of these models is to explain relative changes in the erythral monthly RE, i.e., $\Delta ER(YR, MM)RE(Y, M) = 100\% (RE_{ERYT}(YR, MM)(Y, M) - RE_{ERYT}^*(MM)(M)) / RE_{ERYT}^*(MM)(M)$ with the corresponding relative changes in variables X that affect UVR, $\Delta X(YR, MM)(Y, M) = 100\% (X(YR, MM)(Y, M) - X^*(MM)(M)) / X^*(MM)(M)$, where $X(YR, MM)(Y, M)$ is the monthly mean of DG or TCO_3 in year YRY and month MMM and $X^*(MM)(M)$ is the long-term monthly means for month MMM :

$$\Delta ER_K(YR, MM)RE_K(Y, M) = a_K(M) \Delta DG(YR, MM)(Y, M) + b_K(M) \Delta TCO_3(YR, MM)(Y, M) + c_K, \quad (7)$$

where $K=OBS$ (for Mod2) and $ERA5$ (Mod3) are for the regression using the explaining variables from the measurements at Belsk and ERA5 reanalysis, respectively. Finally, the modelled $RE_{ERYT,K}$ value is equal to:

$$RE_{ERYT,K}(YR, MM)(Y, M) = RE_{ERYT,K}^*(MM) \left(1 + \frac{a_K(M) \Delta DG(YR, MM)(Y, M) + b_K(M) \Delta TCO_3(YR, MM)(Y, M) + c_K}{100} \right) \left(1 + \frac{a_K(M) \Delta DG(Y, M) + b_K(M) \Delta TCO_3(Y, M) + c_K}{100} \right), \quad (8)$$

~~Models defined by Eq. (8) were used to compare fluctuations in UVR data in periods with RB and SL501-A measurements relative to the long-term monthly means in these periods, $RE_{ERYT,K}^*(MM)$, that were approximated using the long-term averages of the measured $RE_{ERYT}(YR, MM, DD)$ values for the period 1976–1992 and 1993–2013, respectively. The regression coefficients, a_K , b_K , and c_K , which were calculated using the standard least-squares linear fit to the most reliable (2014–2023) data (Table 3), were applied to construct monthly time series for the entire measurement period (1976–2023).~~

Table 3. Coefficients of the multilinear regressions derived for each calendar month based on the explaining variables from the measurements at Belsk (Mod2) and ERA5 reanalysis (Mod3) data for the period 2014–2023.

Month:	Mod-2Mod2			Mod-3Mod3		
	a_{OBS}	b_{OBS}	c_{OBS}	a_{ERA5}	b_{ERA5}	c_{ERA5}
January	0.84	–0.77	–5.69	1.34	–1.22	–8.38
February	0.81	–1.12	–0.12	0.95	–1.40	–0.05

March	0.59	-0.93	-0.65	0.84	-0.98	-0.77
April	0.90	-0.85	-1.94	1.26	-1.22	-3.77
May	0.86	-2.00	1.14	0.86	-1.97	0.64
June	1.08	-0.87	-0.05	1.14	-0.83	0.11
July	0.69	-0.84	0.00	0.40	-0.99	-0.00
August	0.82	-1.46	-1.99	0.63	-2.05	-1.40
September	0.86	-0.79	-0.00	0.94	-0.97	-0.00
October	0.80	-1.12	-0.49	0.86	-0.45	-0.52
November	0.58	-1.15	-1.02	0.66	-0.73	-0.97
December	0.73	-0.23	2.11	1.28	2.61	0.77

Models defined by Eq. (8) were used to compare fluctuations in UVR data in periods with RB and SL501A measurements relative to the long-term monthly means in these periods, $RE_{ERYT,K}^*(M)$, that were approximated using the long-term averages of the measured $RE_{ERYT}(Y, M, D)$ values for the period 1976–1992 and 1993–2013, respectively. The regression coefficients, a_K , b_K , and c_K , which were calculated using the standard least-squares linear fit to the most reliable (2014–2023) data (Table 3), were applied to construct monthly time series for the entire measurement period (1976–2023).

2.4 Statistical methods

Several standard statistical characteristics, which are calculated from the relative differences, z_i , between the observed, x_i , and the value of the regression model-value, y_i , values expressed in percentage of the observed value, are used to determine the level of agreement between two time series. These are as follows: mean relative deviation (MRD), mean absolute deviation (MAD), standard deviation (SD), root mean square deviation (RMSD), and Pearson's correlation coefficient (R):

$$z_i = 100\% \frac{y_i - x_i}{x_i}, \quad i = 1, \dots, N, \quad (9)$$

$$MRD = \frac{1}{N} \sum_{i=1}^N z_i, \quad (10)$$

$$MAD = \frac{1}{N} \sum_{i=1}^N |z_i|, \quad (11)$$

$$SD = \left(\frac{1}{N} \sum_{i=1}^N (z_i - MRD)^2 \right)^{\frac{1}{2}}, \quad (12)$$

$$RMSD = \left(\frac{1}{N} \sum_{i=1}^N z_i^2 \right)^{\frac{1}{2}}, \quad (13)$$

$$R = \frac{\sum_{i=1}^N (y_i - \langle y \rangle)(x_i - \langle x \rangle)}{\left(\sum_{i=1}^N (y_i - \langle y \rangle)^2 \right)^{\frac{1}{2}} \left(\sum_{i=1}^N (x_i - \langle x \rangle)^2 \right)^{\frac{1}{2}}}, \quad \langle x \rangle = \frac{1}{N} \sum_{i=1}^N x_i, \quad \langle y \rangle = \frac{1}{N} \sum_{i=1}^N y_i, \quad (14)$$

Standard least-squares linear regression is applied to find the long-term tendency in the data. According to Weatherhead et al. (1998), the standard error of the linear trend estimate, SE_{LS} , by standard least-squares approach should be multiplied by the factor $F = \sqrt{(1 + R_{k+1})/(1 - R_{k+1})}$ to obtain the standard error corrected for the autocorrelation (with a time lag of 1) in the trend residuals, $SE_{LS,COR}$, if the trend residuals are positively correlated with the autocorrelation coefficient equal to R_{k+1} . F is set to 1 if the autocorrelation coefficient in the residual time series is negative.

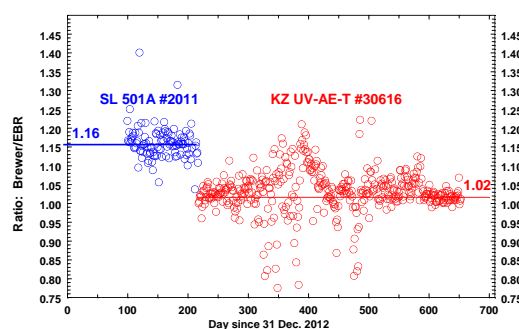
$$SE_{LS,COR} = F \times SE_{LS}, \quad (15)$$

352 Further in the text (~~Section~~Sect. 3.3), the slopes of the regression line will be calculated by Matlab function –
353 $fitlm(x,y)$, and the corrected standard error of the slope, $SE_{LS, COR}$ for cases with $R_{k+1} > 0$, will be enlarged by the
354 factor proposed by ~~Weatherhead~~Weatherhead et al. (1998) (see Eq. (15)).
355

3 Results

3.1 The re-evaluation of the UVR measurements since 5 August 2013

On 5 August 2013, the data of KZ616 replaced the raw SL501A data of SL501A #2011, which had been routinely used for UVR monitoring since 1995, as its performance had deteriorated (Fig. 2). Following this change, a new correction procedure for the Belsk's UVR meter was introduced for early detection of instrument failure. Each month its output (erythemal irradiance) was compared with the corresponding output of the collocated BS64. An example of such a monthly comparison (for June 2023) is shown in the scatter plot between the BS64 and KZ616 erythemal irradiances measured under clear-sky conditions (Fig. 3a). In addition, Fig. 3b shows the monthly mean ratios between these clear-sky BS64 and KZ616 erythemal irradiances for the entire BS and KZ comparison period (irradiance obtained during cloud-free periods from 2014 to 2023).



comparison period (irradiance obtained during cloud-free periods from 2014 to 2023).

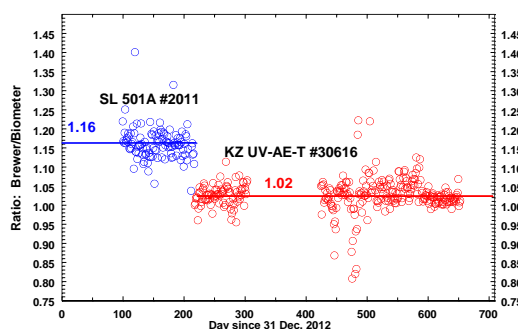


Figure 2. The ratio between the erythemal DRE from the erythemal radiometers (SL501A #2011 before 5 August 2013 and KZ616 afterwards) and the Brewer Mark II spectrophotometer for the 2013–2014 period. The horizontal lines denote the mean value of the ratio.

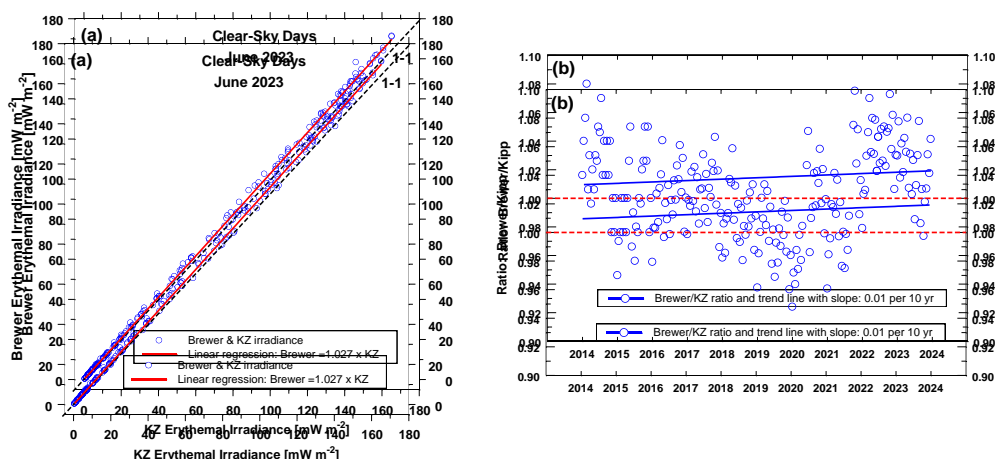


Figure 3. Comparison of the BS64 and KZ616 erythral data for the period 2014–2023: (a) the erythral irradiances measured by the BS64 versus corresponding output of ~~KZ-616~~**KZ616** in June 2023 for clear-sky days, (b) time series of the monthly average of BS64/KZ616 ratios. The dashed line in Fig.3a shows the ideal 1:1 line.

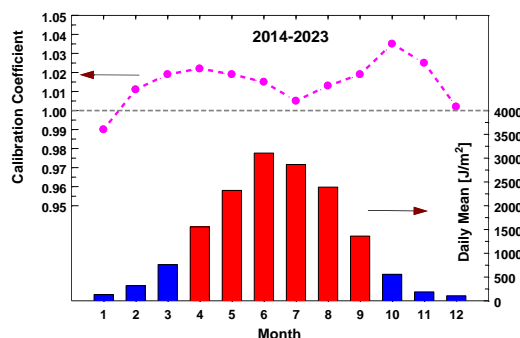
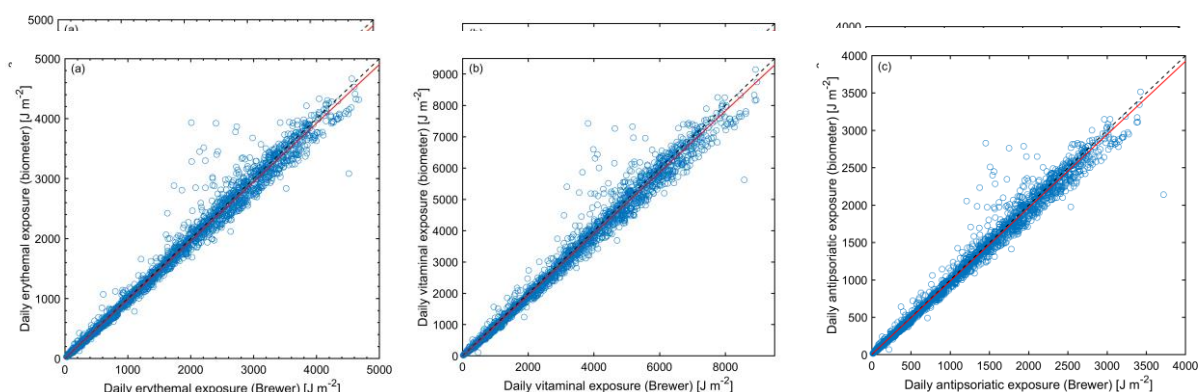


Figure 4. Seasonal pattern of the correction coefficient (CC1) and daily erythral RE for the period 2014–2023. Given Red bars denote months contributing mostly to the annual RE.

The long term (2014–2023) means of the monthly CC1 and erythral DRE for each calendar month are shown in the upper and lower graphs of Fig. 4. The CC1 values are in the range of 1.00 to 1.02 during the period



(April–September) when the intensity of solar UVR is usually high and the fine weather often allows prolonged outdoor activity. Given this and the insignificant trend in the time series of the monthly BS64/KZ ratios (Fig. 3b), it was decided to keep the original KZ616 data without additional adjustments. This assumption is also supported by the BS64/KZ616 comparisons as shown in the scatter plots of Fig. 5, which indicate that the Brewer and EBRBE data cluster about the ideal 1:1 line. For the daily vitamin D₃ and antipsoriatic RE, the values were reconstructed from the daily erythral RE using the transfer coefficients defined by Eq. (4) (the values are archived in the IG PAS Data Portal, Krzyścin (2024)), but the corresponding Brewer values were calculated from the real measured spectra weighted with the action spectra shown in Fig. 1.

Figure 5. Scatter plots (KZ616 versus BS64) for biologically effective DRE in the period 2014–2023: (a) erythema, (b) previtamin D₃ synthesis, and (c) psoriasis clearance.

Additional support for keeping the KZ616 data without a correction provide Fig. 5 where the long-term (2014–2023) means of the monthly CC1 and erythemat DRE for each calendar month are shown in the upper and lower graphs of Fig. 5. The CC1 values are in the range of 1.00 to 1.02 during the period (April–September) when the intensity of solar UVR is usually high and the fine weather often allows prolonged outdoor activity

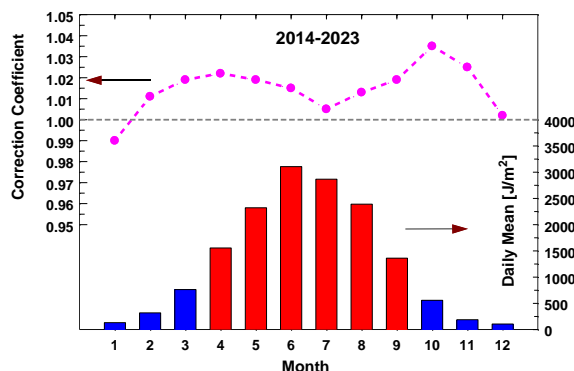


Figure 5. Seasonal pattern of the correction coefficient (CC1) and daily mean of erythemat RE for the period 2014–2023. Red bars denote months contributing mostly to the annual RE.

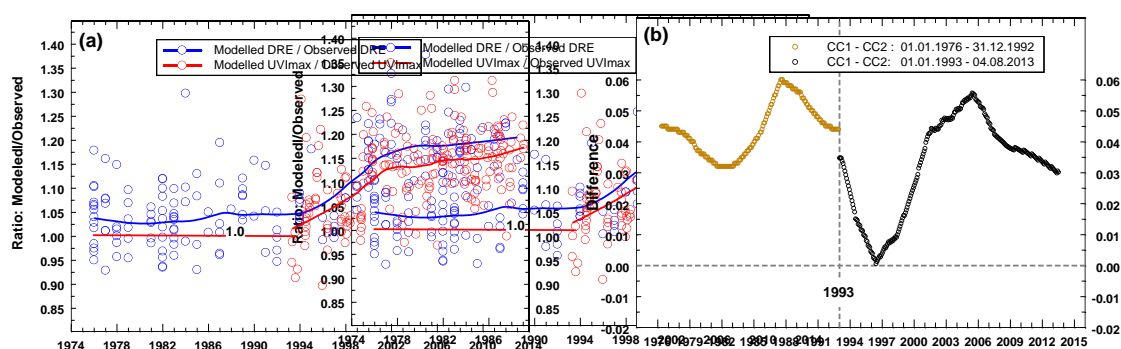
Table A1 shows the values of the descriptive statistics for the period 2014–2023 according to the different ranges of SZA values at local solar noon (SZA_N), which confirm the good agreement between the DRE for all considered biological effects from the well-calibrated BS64 and KZ616 measurements used in routine UVR monitoring. For example, regardless of the biological effect, MRD and RMSD are $\sim -1\%$ and $\sim 9\%$ for $SZA_N < 45^\circ$, which occurs from 8 April to 5 September at Belsk, i.e. during the period with the highest UVR intensity of the year. For $SZA_N \geq 60^\circ$ (from 15 October up to 27 February of next year), MRD and RMSD are only slightly larger ($\sim -2\%$ and $\sim 10\%$, respectively) for the erythema and antipsoriatic exposures. These values are higher ($\sim -13\%$ and $\sim 18\%$) for the previtamin D_3 exposures, raising questions about the usefulness of the erythema radiometers for measuring vitamin D_3 exposure when $SZA_N \geq 60^\circ$. However, vitamin D_3 synthesis in the skin ceases during this period.

3.2 The re-evaluation of the UVR measurements before 5 August 2013

3.2.1 Correction coefficients from the clear-sky model simulations

Analyses of intraday UVR measurements in Belsk from 1 January 1976 to 4 August 2013 have to be divided into two parts, i.e. 1 January 1976–31 December 1992, and 1 January 1993–4 August 2013, due to the different broadband instruments used for UVR monitoring. In the first period, daily erythemal exposures were archived on the basis of manual summation of RB counts per day. For the latter period, 1-min erythemal irradiances were automatically recorded by a logger using [SL501-ASL501A](#) biometers and utilized in the calculation of UVI_{MAX} and daily erythemal RE. Two methods of data correction were proposed (Sect.-2.3.2) using clear-sky data: modelled and measured daily erythemal RE (for the period 1976-2013) and UVI_{MAX} (1993-2013) for the correction method denoted CC1 and CC2, respectively. Figure 6a shows the time series of CC1 and CC2 values together with their smoothed values by the LOWESS smoother, which were used as multipliers of the raw UVR data before 5 August 2013. The difference between CC1 and CC2 are shown in Fig. 6b.

In the 1976-1992 period, UVI values were not archived between 1976 and 1992. This means that CC2 values cannot be directly calculated directly. However, CC2 values were assumed to be equal to 1 could be assumed as the output of because the RB instrument meter was previously adjusted to that by SL501-A the SL501A #927 output using their simultaneous measurements fortaken during the period 1992–1994 period (Puchalski et al., 1995). Such an assumption can also be supported here by a small jump (~1%) in the difference between the CC1 and CC2 values in January 1993 (Fig. 6b). This jump is really small taking into account that the 1993 adjustment of RB



meter was Prior to 1992, CC2 = 1 could be inferred from field comparisons between RB and SL501 A #927 but here this is calculated from smoothing ratios between modelled and observed UVI at noon for clear sky days. Moreover, in the period 1976–1992, an oscillation with 0.015 amplitude is seen around the constant level of CC1=1.045 which justifies the assumption of an almost constant CC2 a flat CC1 pattern before 1993 based on the daily erythemal RE. Using two sets of the re-evaluated 1976–2013 data will allow us to discuss the robustness of trend calculations for the entire 1976–2023 period of the UVR measurements at Belsk (Sect.-3.3).

Figure 6. (a) TUV model-observation ratios for erythemal DRE and noon UVI/UVI_MAX obtained for clear-sky days. The solid curves represent smoothed values of the ratios to be used as the correction coefficients, i.e., the multipliers applied to the raw measurements. The multipliers were set equal to 1 for the 1976–1992 correction based on ratios of noon UVIs, (b) difference between the monthly means of the correction coefficients shown in Fig. 6a.

3.2.2 Performance of the regression models

Erythral DRE for the period 1 January 1976 – 4 August 2013 were reconstructed with Mod1 defined by Eqs. (5–6). The model’s constants came from the model training using the ~~original~~-KZ data and the explaining variables (TCO₃ and DCI) from 5 August 2013 – 31 December 2023 period. The reconstructed values were compared with two sets of the re-evaluated data obtained before 5 August 2013 after multiplying raw daily erythral RE with CC1 and CC2, respectively.

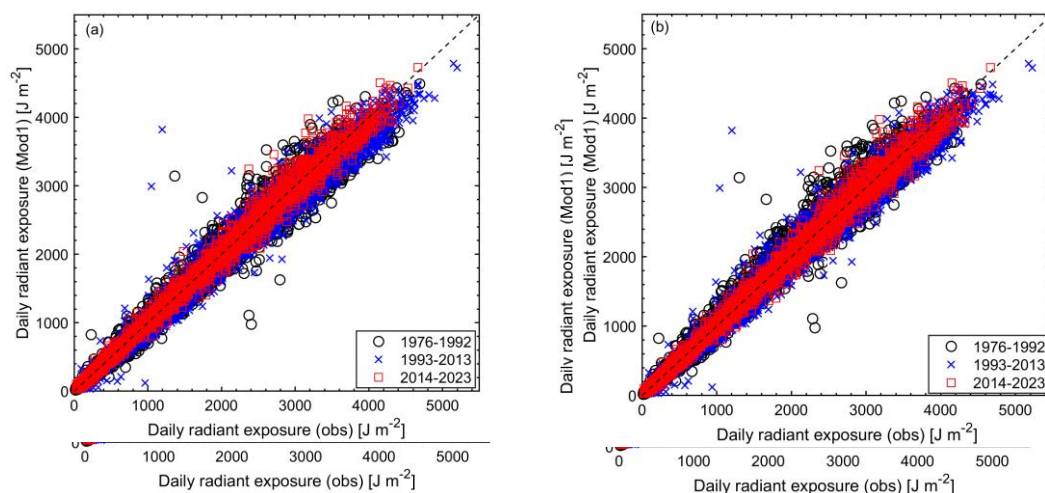


Figure 7. Scatter plot of the modelled (Mod1)– erythral DRE versus the re-evaluated observed values for the 1976–1992, 1993–2013, and 2014–2023 period, respectively: (a) CC1 version of the correction coefficients ~~for the period 1 January 1976–4 August 2013~~, (b) corresponding CC2 version of the correction coefficients. KZ616 measurements were taken without corrections.

Figure 7 shows the scatter plot of the reconstructed (Mod1) versus re-evaluated erythral DRE with CC1 (Fig. 7a) and CC2 (Fig. 7b) multipliers of the raw data for the three periods corresponding to the RB, SL501A, and KZ616 measurements, respectively. The points in Figure 7 cluster around a line of perfect 1-1 agreement with only a few outliers. It seems that there is only a small difference between the re-evaluated daily erythral RE and the corresponding output of Mod1 with the CC1 and CC2 multipliers. This is also supported by similar values of the descriptive statistics for the periods 1976–1992 and 1993–2013 (Table 4). It is worth mentioning that the performance of Mod1 in the period 2014–2023 is similar to that of the Brewer spectrophotometer that was found when compared with the ~~original~~-KZ616 data (note the close values of the descriptive statistics for the ~~year-~~~~found~~~~summer~~ data in column “CC=1” of Table 4 and Table A1 for the “~~AH-SZAN~~”~~“<45°”~~ cell and column “~~ErytERYT~~”, for example, ~~RMSD~~~~MAD~~ values are equal to ~~10.5.2~~ % and ~~8.95.3~~ %, respectively).

Table 4. The descriptive statistics (MRD, MAD, RMSD, and SD) calculated from the relative daily differences, 100% (Mod1 value – re-evaluated measurement)/(re-evaluated measurement), for the periods 1976–1992, 1993–2013 and 2014–2023. The correlation coefficient R was obtained from the re-evaluated measurements and modelled values. Two versions of the re-evaluated datasets were considered, using CC1 and CC2 multipliers on the raw measurements. ~~Both datasets include raw~~For the period 2014-2023, KZ616 data ~~as there was no need to recalculate these data used, which did not require adjustment.~~ The results are shown for annual (January–December) and summer (June–August) data.

Statistics	Year-Round (January–...–December)					June–July–August				
	Multipliers of the raw data									
	1976–1992	1976–1992	1993–2013	1993–2013	2014–2023	1976–1992	1976–1992	1993–2013	1993–2013	2014–2023
	CC1	CC2	CC1	CC2	CC=1	CC1	CC2	CC1	CC2	CC=1
MRD	–2.7	1.6	–1.9	–0.3	1.4	–0.8	3.5	–2.6	–1.0	0.9
MAD	9.8	9.6	9.7	9.4	6.8	7.8	8.1	7.0	6.4	5.2
RMSD	13.7	14.1	14.5	14.6		10.8	11.7	10.1	9.7	6.9

R	1.00	0.99	1.00	0.99	10.5	0.96	0.96	0.97	0.98	0.98
SD	13.4	14.0	14.3	14.6	1.00	10.9	11.2	9.8	9.7	6.8
					10.4					

Erythemat DRE by Mod1 can be obtained for days when the explanatory variables, TCO₃ and DCI, are available from the collocated measurements at Belsk by the Dobson radiometer and pyranometer, respectively. It is therefore possible to fill gaps in the measured data and obtain a complete (1976–2023) series of erythemat DRE to be used in calculations of erythemat annual and summer (June–July–August) RE. These REs can also be calculated using the erythemat monthly RE based on Mod2 and Mod3. All these series are analysed in [Section Sect. 3.3](#) for trend calculations to assess the level of uncertainty in the long-term variability of the Belsk UVR data.

Table 5 shows the values of the descriptive statistics for the three models used (Mod1, Mod2 and Mod3) and two versions of the re-evaluated data (using CC1 and CC2 multipliers on the raw data) based on the annual and summer RE. The differences between descriptive statistics (MRD, MAD, RMSD, SD) in CC1 and CC2 columns are within a few percentage points for MRD and about 1–1.5 percentage points for other statistics, indicating that the different correction methods give fairly similar results. ~~The performance of In most cases, Mod2 and Mod3 is in most cases slightly better than that of outperform~~ Mod1 (see Table 5), with smaller values of descriptive statistics. This is because these models ~~add fluctuations to the mean values are based on relative monthly differences from the respective long-term means~~ for the periods 1976–1992, 1993–2013 and 2014–2023 ~~calculated from the~~. These means were obtained by averaging the re-evaluated ~~measurements of RB, meter and SL501A (#919 and #2011 for the periods 1993–1994, and 1995–2013 respectively) and the original the KZ616 measurements data. The Mod1 model did not apply a constraint on the average UVR in these sub-periods.~~

All models considered were designed to test whether changes in the primary UVR drivers, ozone and clouds, explain year-to-year UVR variability. The performance of Mod3 is surprisingly similar to that obtained from Mod2 despite the use of UVR proxies (TCO₃ and DGI) from the ERA5 reanalysis.

The ~~lowestsmallest~~ correlation coefficients between the re-evaluated measurements and modelled values were found in the period 1993–2013 for the measurement-model pairs with the same version of the CC multipliers (CC1 or CC2). This is particularly pronounced for the summer data (see e.g. Mod3 values of 0.50 and 0.43 for CC1 and CC2 pairs, respectively), suggesting a poorer agreement between measurements and model in the period 1993–2013. This was found for all models. However, other descriptive statistics (MRD, MAD, RMSD and SD) differed only slightly, i.e. ~~less than~~ 1.5 percentage points, when values in CC1 and CC2 columns were compared.

Table 5. Same as Table 4, but the descriptive statistics are calculated using time series of erythemat annual and summer RE.

Statistics	Year-Round: January–...–December					Summer: June–July–August				
						Multipliers of the raw data				
	1976–1992		1993–2013		2014–2023	1976–1992		1993–2013		2014–2023
	CC1	CC2	CC1	CC2	CC=1	CC1	CC2	CC1	CC2	CC=1
	Mod1									
MRD	–3.3	0.9	–4.2	–2.6	–0.2	–1.9	2.4	–3.5	–1.9	0.5
MAD	3.9	2.5	4.7	3.2	1.0	4.0	3.4	4.4	2.8	1.8
RMSD	4.4	2.9	5.0	3.5	1.2	4.4	4.5	4.8	3.4	2.6
R	0.82	0.86	0.77	0.83	0.93	0.92	0.93	0.57	0.65	0.96
SD	3.2	3.0	2.8	2.4	1.4	4.2	4.0	3.3	2.9	2.7
	Mod2									

MRD	-0.9	-1.0	-0.5	-0.6	-0.3	-1.0	-1.1	-0.6	-0.6	0.0
MAD	2.1	2.0	2.0	1.8	0.6	3.3	2.9	2.2	1.9	1.3
RMSD	2.6	2.4	2.7	2.3	0.8	4.0	3.7	2.8	2.4	1.8
R	0.90	0.92	0.81	0.86	0.97	0.93	0.94	0.72	0.79	0.98
SD	2.6	2.4	2.7	2.3	0.8	4.1	3.7	2.8	2.4	1.9
Mod3										
MRD	-0.4	-0.5	-0.9	-0.9	-0.6	0.2	0.1	-0.3	-0.3	0.1
MAD	1.5	1.4	2.7	2.8	0.8	3.0	3.2	2.9	2.9	2.1
RMSD	1.7	1.9	3.4	3.6	0.9	3.7	3.7	3.7	3.7	2.5
R	0.96	0.94	0.70	0.67	0.97	0.94	0.94	0.50	0.43	0.92
SD	1.8	2.0	3.4	3.5	0.8	3.9	3.9	3.8	3.8	2.7

3.3 Trend analyses

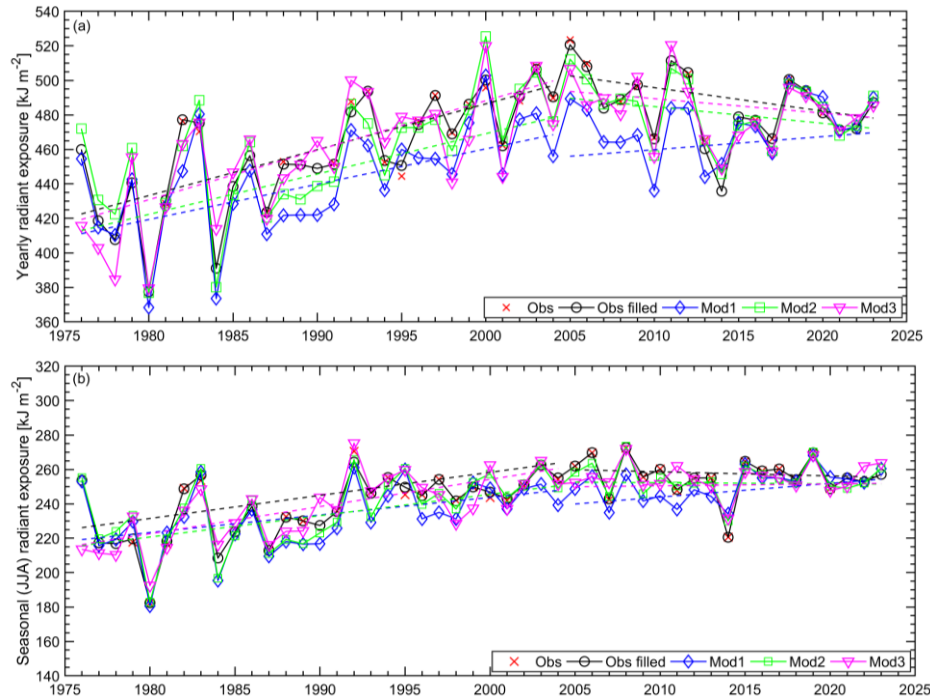
3.3.1 The erythema annual and summer radiant exposures in the period 1976-2023

Trend analyses are applied to the erythema annual and summer RE based on daily RE. There are two series to be considered when dealing with the measured data. The first, labelled OBS, uses only re-evaluated observations and the monthly average is calculated when at least 14 daily ERE values are available. The second one, OBS_F, contains all the daily gaps filled by Mod 1 simulations. For other models used there are no gaps. In the case of Mod1, the erythema annual and summer RE are ~~built constructed~~ using the ~~re-evaluated daily ERE results of the TUV model~~ and the CMFs estimated from the DCI values. For Mod2 and Mod3, the monthly reconstructed RE values are summed over the year and summer season.

The 1976–2023 time series for the erythema annual and summer RE using CC1 and CC2 correction multipliers are shown in Fig. 8 and Fig. A1, respectively. Fig.8a (~~Fig.A1a~~) and Fig.8b (~~Fig.A1b~~) are for the erythema annual (and summer) RE ~~with the use of CC1 but correspondingly Fig.A1a and Fig.A1b are based on CC2 values.~~

Linear regression lines are superimposed on the graphs to illustrate the long-term variability in the time series. Two independent lines are drawn to account for a change in the trend pattern observed in the time series somewhere in the early 2000s. The year of the trend change was calculated by examining the performance of fifteen combinations of this two-line pattern, varying the year of the trend change point (from 1995 to 2009). The best fit with maximum coefficients of determination was found for the trend change point in 2005. Therefore, the slopes of the regression lines (in kJ m⁻² per year) and the trend values (in % per year) shown in Table 6 and Table 7, respectively, are calculated for the 1976–2004 and 2005–2023 periods. Standard errors of the trend estimates are calculated according to Eq. (15) accounting for the correction for the autocorrelation in the trend residuals if the autocorrelation coefficient with 1-yr lag, R_{k+1} , is positive (also shown in Tables 5–6).

The interannual variations and trend lines of erythral annual RE are close to each other when comparing the upper graphs in Fig. 8 and Fig.A1. This can also be observed for the summers when comparing the corresponding lower plots. At the beginning of the RB observations (1976–1986), there were large oscillations from year to year, suggesting an instrumental problem with the data. ~~However, all modelled time series show quite similar oscillations for this period, supporting the hypothesis that a specific combination of TCO₂ and cloud transparency may be responsible for such oscillations.~~ As TCO₂ and cloud transparency data are available, it is important to



~~analyse whether these large fluctuations are due to one or both of these two factors.~~

~~Figure 8. Time series (1976–2023) of the erythral radiant exposures from re-evaluated observations (Obs), re-evaluated observations with filled gaps (Obs filled), and model estimates (Mod1, Mod2, and Mod3) using the CC1 version of the correction coefficient: (a) annual (January–December) radiant exposures; (b) summer (June–August) radiant exposures. Dashed lines represent the linear trends calculated for the period 1976–2004 and 2005–2023.~~

The slopes of the linear fit to the analysed time series (Table 6) show a statistically significant positive trend between 1976 and 2004 of around 20–30 kJ m⁻² and 10–20 kJ m⁻² per decade in the annual and summer data, respectively. The trends are mostly insignificant for the period 2005–2023, with only one exception (for the Mod1 data) with a continued positive trend of ~ 10 kJ m⁻² per decade. The corresponding trend values expressed in dimensionless units (Table 7) have the same values of about 4–7% per 10 years in the former period for both the annual and summer time series. In the latter period, the positive summer trend ~~offrom~~ Mod1 is ~3 % per 10 years. Mod 1 and Mod 3 (with CC2) gave the lowest and highest trends, respectively. However, the differences between these trends are within the range of ~~± 2 standard errors the uncertainty~~ of the trend estimates, ~~taking into account the autocorrelation in at the residuals of the models (column 95% confidence level (as given by T_cSE_{LS, COR} values~~ in Table 6).

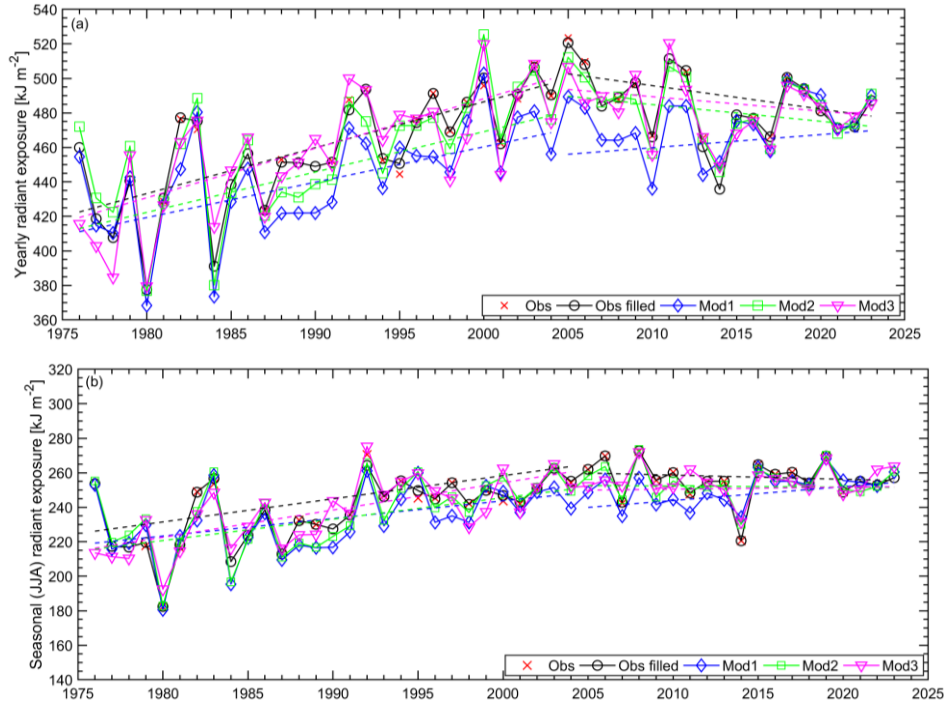


Figure 8. Time series (1976–2023) of the erythemal radiant exposures from re-evaluated observations (Obs), re-evaluated observations with filled gaps (Obs filled), and model estimates (Mod1, Mod2, and Mod3) using the CC1 version of the correction coefficients: (a) annual (January–December) radiant exposures; (b) summer (June–Aug) radiant exposures. Dashed lines represent the linear trends calculated for the period 1976–2004 and 2005–2023.

By averaging all available statistically significant annual and summer trend values shown in the third and seventh columns of Table 6 and Table 7, the following trends and their standard errors are obtained: for the period 1976–2004: $27.4 \pm 4.4 \text{ kJ m}^{-2}$ and $5.64 \pm 0.92 \%$ per decade for the erythemal annual RE, and $14.3 \pm 4.3 \text{ kJ m}^{-2}$ and $5.63 \pm 1.03 \%$ per decade for the erythemal summer RE. These values correspond to the average trend from the two series based only on the re-evaluated measurements (OBS_F values in the Tables), i.e. 28.7 kJ m^{-2} and 5.9% per decade for the erythemal annual RE, and 14.3 kJ m^{-2} and 5.6% per decade for the erythemal summer RE.

Table 6. Trends (kJ m^{-2} per year) by the linear least-squares fit to the time series of erythemal annual and summer radiant exposures shown in Fig.8 and Fig.A1 calculated for the periods 1976–2004 and 2005–2023. SE_{LS, COR} denotes the standard error of the trend estimate taking into account the autocorrelation R_{k+1} (with a lag of 1 year) in the series of the residuals of the trend model. R_{k+1} denotes the correlation coefficient in the lagged residuals. Bold font indicates a statistically significant trend value at the 2-sigma 95% confidence level, based on the standard error of the trend multiplied by the corresponding critical T-value (T_c) for a two-sided probability. For the periods 1976–2004 and 2005–2023, T_c is 2.05 and 2.10, respectively, with 28 and 18 degrees of freedom.

Data	Correct.	Annual (January...–...December) sum [kJ m ^{−2}]				Summer (June–July–August) sum [kJ m ^{−2}]			
Type	Method	Trends _{1976–2004}		Trends _{2005–2023}		Trends _{1976–2004}		Trends _{2005–2023}	
		Trend ±	R _{k+1}	Trend ±	R _{k+1}	Trend ±	R _{k+1}	Trend ±	R _{k+1}
		<u>T_cSE_{LS}, COR</u>		<u>T_cSE_{LS}, COR</u>		<u>T_cSE_{LS}, COR</u>		<u>T_cSE_{LS}, COR</u>	
OBS _F	CC1	2.66 ±0.521.07	−0.11	−1.36 ±0.982.06	0.17	1.34 ±0.3776	0.08	−0.24 ±0.491.03	−0.32
	CC2	3.08 ±0.521.07	−0.06	−0.45 ±0.871.83	0.14	1.52 ±0.3776	0.07	−0.26 ±0.481.01	−0.30
Mod1	–	2.05 ±0.571.17	−0.19	0.76 ±0.781.64	0.08	1.02 ±0.3878	−0.13	0.80 ±0.3676	−0.20

Mod2	CC1	2.34 ±0.61 <u>1.25</u>	-0.16	-0.97 ±0.85 <u>1.78</u>	0.12	1.24 ±0.39 <u>0.80</u>	-0.08	-0.06 ±0.41 <u>86</u>	-0.38
	CC2	2.84 ±0.61 <u>1.25</u>	-0.10	-0.30 ±0.79 <u>1.66</u>	0.10	1.50 ±0.39 <u>0.80</u>	-0.01	0.29 ±0.41 <u>86</u>	-0.32
Mod3	CC1	2.84 ±0.56 <u>1.15</u>	-0.21	-0.84 ±0.76 <u>1.60</u>	-0.08	1.58 ±0.32 <u>0.66</u>	0.02	0.11 ±0.37 <u>78</u>	-0.13
	CC2	3.34 ±0.54 <u>1.11</u>	-0.22	-0.17 ±0.72 <u>1.51</u>	-0.13	1.82 ±0.20 <u>0.41</u>	0.05	0.46 ±0.36 <u>76</u>	-0.13

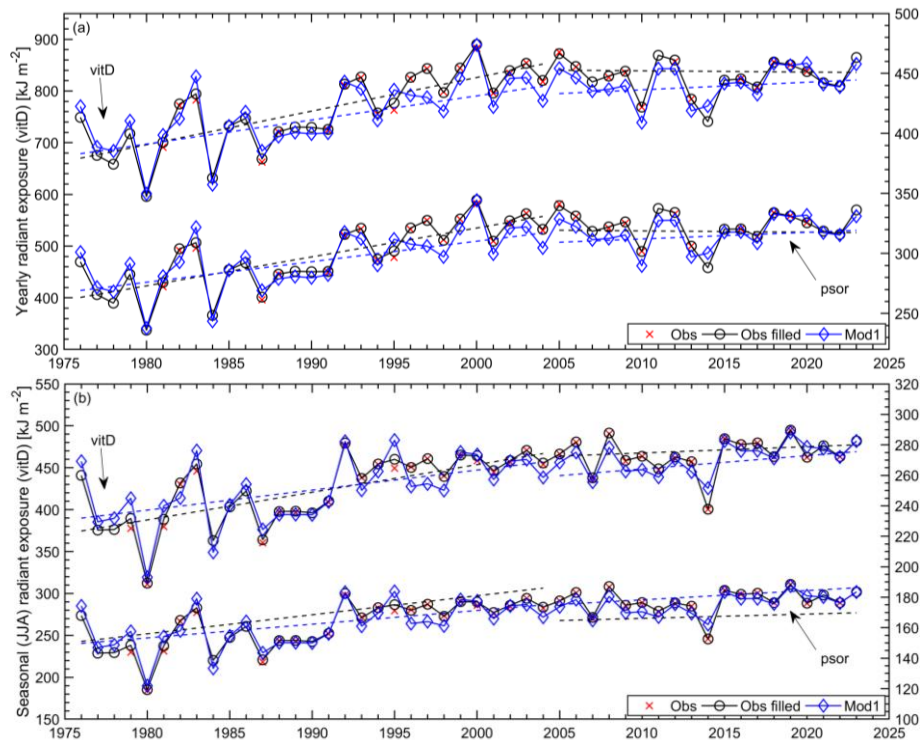
Table 7. Same as Table 6, but the results are for the trend values expressed in % per year.

Data Type	Correct. Method	Annual (January...December) sum [% yr ⁻¹]				Summer (June–July–August) sum [% yr ⁻¹]			
		Trends _{1976–2004}		Trends _{2005–2023}		Trends _{1976–2004}		Trends _{2005–2023}	
		Trend ±	R _{k+1}	Trend ±	R _{k+1}	Trend ±	R _{k+1}	Trend ±	R _{k+1}
		<u>T_cSE_{LS}, COR</u>		<u>T_cSE_{LS}, COR</u>		<u>T_cSE_{LS}, COR</u>		<u>T_cSE_{LS}, COR</u>	
OBS _F	CC1	0.54 ±0.11 <u>0.22</u>	-0.11	-0.28 ±0.17 <u>0.36</u>	0.17	0.52 ±0.14 <u>0.29</u>	0.08	-0.09 ±0.19 <u>0.40</u>	-0.32
	CC2	0.64 ±0.11 <u>0.22</u>	-0.06	-0.09 ±0.16 <u>0.34</u>	0.14	0.60 ±0.14 <u>0.29</u>	0.07	0.10 ±0.19 <u>0.40</u>	-0.30
Mod1	–	0.42 ±0.12 <u>0.25</u>	-0.19	0.16 ±0.15 <u>0.31</u>	0.08	0.40 ±0.15 <u>0.31</u>	-0.13	0.31 ±0.14 <u>0.29</u>	-0.20
Mod2	CC1	0.48 ±0.13 <u>0.27</u>	-0.16	-0.20 ±0.15 <u>0.31</u>	0.12	0.49 ±0.15 <u>0.31</u>	-0.08	-0.02 ±0.16 <u>0.34</u>	-0.38
	CC2	0.59 ±0.12 <u>0.25</u>	-0.10	-0.06 ±0.15 <u>0.31</u>	0.10	0.59 ±0.15 <u>0.31</u>	-0.01	0.11 ±0.16 <u>0.34</u>	-0.32
Mod3	CC1	0.59 ±0.12 <u>0.25</u>	-0.21	-0.17 ±0.16 <u>0.34</u>	-0.08	0.62 ±0.12 <u>0.25</u>	0.02	0.04 ±0.15 <u>0.31</u>	-0.13
	CC2	0.69 ±0.11 <u>0.22</u>	-0.22	-0.04 ±0.15 <u>0.31</u>	-0.13	0.72 ±0.13 <u>0.27</u>	0.05	0.18 ±0.14 <u>0.29</u>	-0.13

3.3.2 The vitamin D₃ and antipsoriatic annual and summer radiant exposures in the period 1976-2023

The commercial EBRs used to monitor erythral irradiance can also measure non-erythral irradiance (Czerwińska and Krzyścin, 2024a). Figure 54 and Table A1 provide that the daily vitamin D₃ and antipsoriatic RE derived from the KZ616 measurements agree with the directly measured BS64 values ~~in, as are the same way as the original (erythral) data obtained with KZ616 data.~~ This supports the method of the transfer from erythral irradiance to non-erythral irradiance proposed by Czerwińska and Krzyścin (2024a).

Figure 9 shows the time series of annual and summer values of previtamin D₃ synthesis and psoriasis healing RE from 1976 to 2023. It appears that these time series are very similar. In addition, these time series are similar to the erythral series shown in Fig.8. The correlation coefficients between the pairs of time series shown in Fig.8 and Fig.9, i.e. erythema & vitamin D₃, erythema & psoriasis, vitamin D₃ & psoriasis, were in the range [0.90, >0.999] with the lowest value for the erythema & vitamin D₃ and erythema & psoriasis pairs when the summer data from Mod1 simulations were considered.



565
566
567
568
569

Figure 9. Time series (1976–2023) of the previtamin D₃ synthesis and psoriasis healing radiant exposures from re-evaluated observations (Obs), re-evaluated observations with filled gaps (Obs filled), and model Mod1 estimates (Mod1) using the CC2 version of the correction coefficients: (a) annual (January–December) radiant exposures; (b) summer (June–July–August) radiant exposures. Dashed lines represent the linear trends calculated for the period 1976–2004 and 2005–2023.

570
571
572
573
574
575
576

Table 8 shows the trend values for the period 1976–2004 and 2005–2023 from the time series calculated using the erythemal DRE multiplied by the transfer coefficients defined by Eq. (4). The transfer coefficients depend on only two parameters (TCO₃ and SZA), even on cloudy days, as previously shown by Czerwińska and Krzyścin (2024a). The statistically significant trend values for previtamin D₃ synthesis and psoriasis clearance are slightly higher, by about 1–1.5 percentage points per decade, than the corresponding trend values for the erythema shown in Table 7. Taking into account the ~~standard error uncertainty~~ of the trend estimate of about ~~+3~~ % per decade, it cannot be said that the differences between the trends are statistically significant.

577 **Table 8.** Same as Table 7, but trend values are for previtamin D₃ synthesis and psoriasis clearance.

Data Type	Correct. Method	Annual (January–December) RE [% per year]				Summer (June–July–August) RE [% per year]			
		Trends _{1976–2004}		Trends _{2005–2023}		Trends _{1976–2004}		Trends _{2005–2023}	
		Trend ±	R _{k+1}	Trend ±	R _{k+1}	Trend ±	R _{k+1}	Trend ±	R _{k+1}
		<u>T_c</u> SE _{LS} , COR		<u>T_c</u> SE _{LS} , COR		<u>T_c</u> SE _{LS} , COR		<u>T_c</u> SE _{LS} , COR	
Previtamin D ₃ synthesis									
OBS _F	CC1	0.70 ±0.1225	−0.12	−0.27 ±0.2246	0.12	0.64 ±0.1633	0.06	−0.07 ±0.2042	−0.25
	CC2	0.77 ±0.1225	−0.07	−0.03 ±0.1940	0.08	0.71 ±0.1531	0.05	0.16 ±0.1940	−0.32
Mod1	–	0.56 ±0.1429	−0.20	0.17 ±0.1634	0.02	0.51 ±0.1633	−0.15	0.34 ±0.1429	−0.18
Psoriasis clearance									
OBS _F	CC1	0.66 ±0.1225	−0.13	−0.27 ±0.2144	0.15	0.63 ±0.1531	0.06	−0.07 ±0.2042	−0.25

	CC2	0.74 ±0.1225	-0.08	-0.03 ±0.2042	0.10	0.70 ±0.1531	0.05	0.16 ±0.1940	-0.26
Mod1	-	0.53 ±0.1327	-0.20	0.17 ±0.1838	0.14	0.51 ±0.1633	-0.15	0.34 ±0.1429	-0.18

4 Summary and Discussion

Belsk is a unique observatory where UVR monitoring has been accompanied by monitoring of ozone (TCO₃), aerosol optical properties (AOD) and cloud characteristics (sunshine duration, DCI from global solar irradiance measurements), i.e. basic input parameters to a radiative transfer model allowing reconstruction of the erythemal RE. In addition, collocated BS64 measurements of UVR spectra are used in the frequent (every -month) checking of actual KZ616 performance. BS64 spectral measurements also allow assessment of the quality of Czerwińska and Krzyścin (2024a) retrieval to convert standard erythemal measurements to the non-erythemal BE irradiance (see the cases of the vitamin D₃ and antipsoriatic DRE in [Figure 5Fig.4](#)).

Two sets of raw UVR data multipliers (CC1 and CC2 as defined in section 2.3.2) have been proposed to ~~assesscorrect and homogenise~~ the ~~uncertainty range~~ ~~time series~~ of ~~the correction method applied to the raw~~ ~~UVRErythemal~~ data. The re-evaluated time series appear quite similar, i.e. the difference between these series is within a few percentage points (Table 4 and Table 5). There was no need to re-evaluate the KS616 data for the period 2014–2023 because they agreed well with the BS64 data (Fig.3 and Fig.[54](#)).

Regression models trained on the KZ616 data for the period 2014–2023 allowed the data to be reconstructed from the beginning of UVR observations at Belsk. These reconstructed series allowed independent examination of the pattern of interannual variability (which was unexpectedly large before 1985) and trends in the erythemal annual and summer RE. The regression models generally mimic the observed long-term variability in the re-evaluated daily erythemal exposures. The statistically significant trend of ~6 % per decade with ~~athe~~ standard error of ~1 % per decade for the period 1976–2005 ~~can be~~ ~~is~~ calculated (for both erythemal annual and summer RE) by averaging trends from the sample of seven versions of trend estimates from re-evaluated and reconstructed data (Table 7). All individual trend values [in Table 7](#) are within the range ~~of the mean trend ±6% ± 2-standard error%~~ (i.e. there is no outlier in this trend sample).

The ~~standard errors for the uncertainty (at the 95% confidence level) of the~~ individual trend estimates [for the period 1976-2005 \(Table 7\)](#) are ~~in the range of 1-1.5~~ ~~about 2-3~~ per decade, i.e. quite close to ~~double~~ the standard error of the ~~averagedmean~~ trend derived from the ~~trend~~-sample. This supports the robustness of the trend estimates in annual and summer RE for the 1976–2005 parts of the Belsk time series. In addition, it also appears that the correction methods applied to the 1976–2013 raw UVR data, based on the comparisons of clear-sky erythemal DRE (CC1 method) and noon UVI (CC2 method), lead to differences in the individual 1976–2005 trend estimates of [only](#) about 1 % per decade (see Table 7 for the trend differences between pairs of OBS_F, Mod2 and Mod3 calculated with the CC1 and CC2 correction applied to the raw time series).

We found that our DRE estimates for all biological effects considered (erythema, vitamin D₃ and psoriasis) were close to those obtained from the Brewer's spectra with ~~a~~ bias of ~ -1 % and a standard deviation of ~ 9 % (Table A1) for the part of the year when UVR is of particular interest, when ~~the-midday~~ ~~SZA~~ [at local solar noon](#) is less than 45° (i.e. below the shadow length), according to the so-called shadow rule for protection against high UVR (Downham, 1998).

Krzyścin et al. (2011) found a trend of $5.6 \% \pm 0.9 \% (1\sigma)$ per decade in the erythema annual RE for the period 1976–2008. This is in good agreement with the present trend estimate, regardless of the very different correction methods used. The correction of the ~~SL501-ASL501A~~ data carried out in 2011 was based on simultaneous measurements with KZ616 for the period 2008–2009 and further corrections for the instrument ageing using TUV cloudless sky simulations.

Similar trend estimates for erythema radiation can be inferred from the reconstructed erythema time series for the Moscow region based on the UVR measurements by the broadband (300–380 nm) radiometer (Chubarova et al., 2018) and the statistically reconstructed erythema radiation series for Hradec Kralowe (Čížková et al., 2018). For the Moscow region, the authors reported a statistically significant positive trend of more than 5 % per decade for the period 1979–2015. Volpert and Chubarowa (2021) revealed the decadal trend in the reconstructed erythema UV irradiance over the Moscow region for the warm season (May–September) of $5.1 \% \pm 1.1 \%$ per decade in the period 1979–2016. Estimates from the smoothed pattern of annual erythema exposures taken from Fig. 2c by Čížková et al. (2018) for 1976 ($\sim 1.20 \text{ kJ m}^{-2}$ for the annual mean of erythema daily RE) and 2005 ($\sim 1.40 \text{ kJ m}^{-2}$) give a trend of $\sim 5\%$ per decade for the period 1976–2004. From around 2005, both time series show a levelling off. Trends calculated here from the RE time series for other biological effects (previtamin D₃ synthesis and psoriasis lesion clearance), using an approach analogous to that used for the erythema data, show very similar trends.

5 Code and data availability

All data have been published as free access TXT files and are made available through PANGAEA repository at <https://doi.org/10.1594/PANGAEA.972139> (Krzyścin et al., 2024) and IG PAS Data Portal repository: https://doi.org/10.25171/InstGeoph_PAS_IGData_Biologically_Effective_Solar_Radiation_Belsk_1976_2023 (Krzyścin, 2024). ERA5 data are publicly accessible at <https://cds.climate.copernicus.eu/datasets/reanalysis-era5-single-levels?tab=overview> (ERA5, 2025). MERRA-2 data are accessible at <https://doi.org/10.5067/Q9QMY5PBNV1T> (GMAO, 2025). Coefficients of the linear regression are calculated by Matlab function (Matlab R2018a) – *fitlm(x,y)*.

6 Conclusions

It is ~~widelygenerally~~ accepted that the use of ~~overlapping measurements a sample of time~~ series ~~from containing~~ different ~~instruments possible realisations of a time series~~ increases the reliability of ~~the~~ results ~~obtained from~~ ~~compared to the analysis of a single time series analyses. Consequently, the inclusion of at least two different time series for analyses of the.~~ Therefore, this study includes 7 time series (refer to number of analysed time series shown in Table 7) to discuss the reliability of year-to-year variability ~~of a selected quantity over the entire measurement period is also and~~ trends in annual and summer biologically effective radiant exposures. This is beneficial for ~~assessing data evaluating the quality of the data~~ and establishing confidence in the results ~~obtained. This is illustrated by the current data.~~ Data archived in ~~the~~ PANGAEA (Krzyścin et al., 2024) and ~~in the~~ IG PASPAN Data Portal (Krzyścin, 2024). ~~The~~, together with the results of three regression models, form the reliable basis for analysing UVR time series at Belsk for the period 1976–2023. The long-term variability of erythema radiation calculated for Belsk corresponds to that previously recorded at distant stations in central/eastern Europe, making results of these future analyses applicable to wider areas. For example, the daily characteristics of BE radiation at

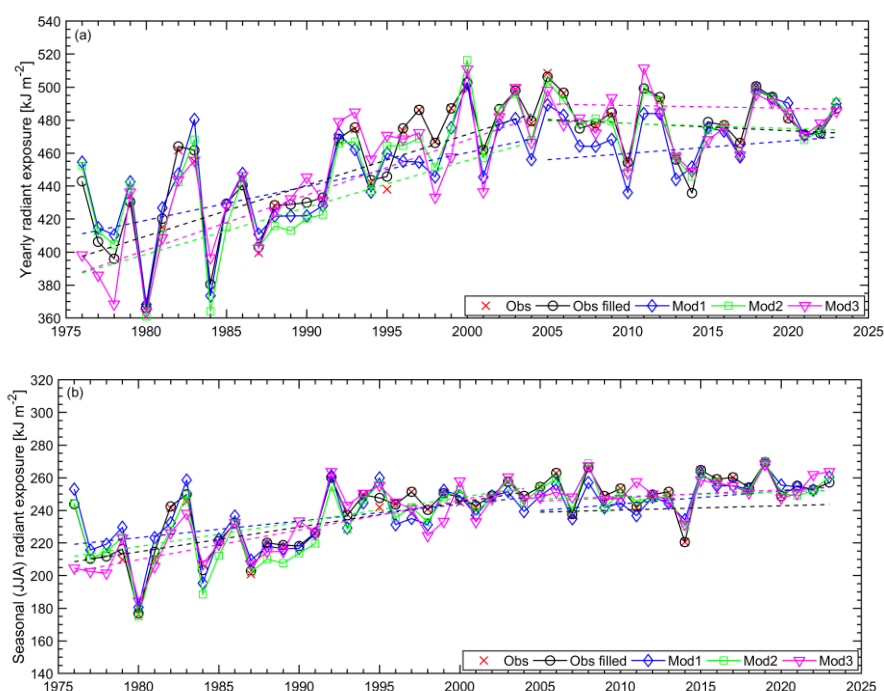
Belsk seem to allow the elaborationdevelopment of scenarios of humanfor outdoor human activities, enabling people to obtain the maximum health benefits from sunbathing while minimising the risk of erythema overexposure. The long term variability of erythema radiation calculated for Belsk corresponds to that previously recorded at distant stations in central/eastern Europe, making these scenarios applicable to wider areas.

Appendix A

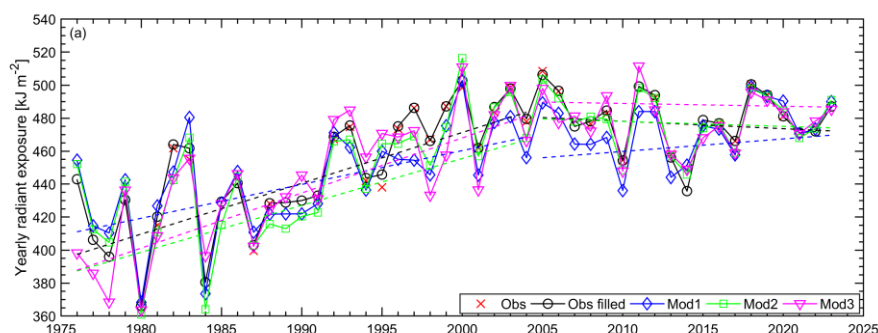
Table A1 presents descriptive statistics (defined in Sect. 2.4) of the relative differences between biologically effective DRE measured by the KZ616 and the BS64, $100\%(RE_{EFF, KZ616} - RE_{EFF, BS64})/RE_{EFF, BS64}$. The vitamin D₃ (VitD) and antipsoriatic (Psor) RE were reconstructed from the erythema (Eryt) RE (Sect. 2.3.3), but the Brewer RE values were calculated using the daily integral of the measured spectral irradiance weighted by the action spectra (Fig.1).

Table A1. Descriptive statistics of the 2014-2023 relative differences between the daily biologically effective radiant exposure with the Kipp & Zonen erythema radiometer (UV-S-AE-T #30616) and the Brewer spectrophotometer #064 in percent of the Brewer data for the different midday-SZA ranges (SZAN), at local solar noon.

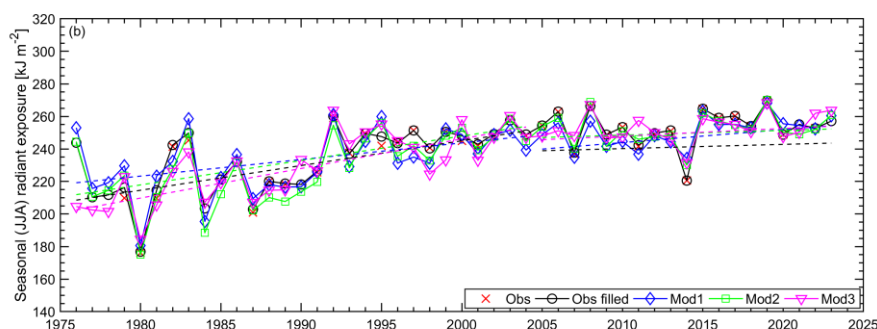
Statistics	SZAN<45°			SZAN [45°, 60°]			SZAN≥60°		All SZAN				
	Ery	VitD	Psor	Ery	VitD	Psor	Eryt	VitD	Psor	Ery	VitD	Psor	
	ER	VIT	PS	ER	VIT	PS	ERYT	VIT	PSO	YT	D	OR	
	YT	D3	OR	YT	D3	OR		D3	R				
MRD	-0.6	-1.5	-0.7	-2.5	-6.6	-3.3	-1.7	-13.2	-1.7	-1.4	-6.8	-1.6	
MAD	5.3	6.0	5.6	4.9	7.9	5.4	6.8	14.7	7.0	5.8	9.6	6.1	
RMS	8.7	9.2	9.0	7.2	10.0	7.8	10.0	16.3	10.3	8.9	12.4	9.3	
SD	8.7	9.1	9.0	6.8	7.6	7.1	9.9	9.5	10.2	8.8	10.4	9.1	



668



669



670 **Figure A1.** Same as Fig.8, but for the re-evaluated observations with the CC2 correction coefficients.

671

672 **Authors contributions.** Conceptualisation, JK and AC; methodology, JK, AC, JJ, PS, and BR; validation, AC
 673 and IP; visualisation, AC; writing (original draft preparation), JK and AC; writing (review and editing), JK, AC,
 674 PS, and IP; funding acquisition, JK and JJ. All authors have read and agreed to the published version of the paper.

675 **Competing interests.** The contact author has declared that none of the authors has any competing interests.

676 **Acknowledgments.** This work was partially financially by the Chief Inspectorate of Environment Protection,
 677 contract number GIOŚ/31/2023/DMŚ/NFOŚ.

678 References

679 AERONET: Aerosol Robotic Network: <https://aeronet.gsfc.nasa.gov/>, last access: 15 April 2025.

680 Berger, D. S.: The sunburning ultraviolet meter: design and performance, *Photochem. Photobiol.*, 24, 587–593,
 681 1976.

682 Blumthaler, M., Ambach, W., Morys, M., and Slomka J.: Comparison of Robertson-Berger UV Meters From
 683 Innsbruck and Belsk, *Publs. Inst. Geophys. Pol. Acad. Sc.*, D-32 (230), 1989.

684

685 Borkowski, J. L.: Reevaluation of series of solar UV-B radiation data, *Publs. Inst. Geophys. Pol. Acad. Sc.*, D-48,
 686 291, 81–89, 1998.

687 Borkowski, J. L.: Homogenization of the Belsk UV-B series (1976–1997) and trend analysis, *J. Geophys. Res.*,
 688 105(D4), 4873–4878, <https://doi.org/10.1029/1999JD900500>, 2000.

689 Borkowski, J.L.: Modelling of UV radiation at different time scales, *Ann. Geophys.*, 26, 3, 441–446,
690 <https://doi.org/10.5194/angeo-26-441-2008>, 2008.

691 Chubachi, S.: Preliminary result of ozone observations at Syowa Station from February, 1982 to January, 1983,
692 *Mem. Natl. Inst. Polar Res., Spec. Issue (Jpn)*, 34, 13–20, 1984.

693 Chubarova, N. Y., and Nezval', Y. I.: Thirty year variability of UV irradiance in Moscow, *J. Geophys. Res.*, 105,
694 12529–12539, <https://doi.org/10.1029/1999JD901192>, 2000.

695 Chubarova, N. E., Pastukhova, A. S., Galin, V. Y., and Smyshlyaev, S. P.: Long-Term Variability of UV Irradiance
696 in the Moscow Region according to Measurement and Modeling Data, *Izv. Atmos. Ocean. Phys.*, 54, 139–146,
697 <https://doi.org/10.1134/S0001433818020056>, 2018.

698 CIE 174:2006: Commission Internationale de l'Eclairage. Action Spectrum for the Production of Previtamin D3
699 in Human Skin. CIE: Vienna, Austria, pp.1–16, 2006.

700 CIE 17166:2019(E): Commission Internationale de l'Eclairage. Erythema Reference Action Spectrum and
701 Standard Erythema Dose. CIE, Vienna, Austria, pp.1-5, 2019.

702 Čížková, K., Láska, K., Metelka, L., and Staněk, M.: Reconstruction and analysis of erythema UV radiation time
703 series from Hradec Králové (Czech Republic) over the past 50 years, *Atmos. Chem. Phys.*, 18, 1805–1818,
704 <https://doi.org/10.5194/acp-18-1805-2018>, 2018.

705 Cleveland, W. S.: Robust Locally Weighted Regression and Smoothing Scatterplots, *J. Am. Stat. Assoc.*, 74 (368),
706 829–836, <https://doi.org/10.1080/01621459.1979.10481038>, 1979.

707 Czerwińska, A., and Krzyścin, J.: Measurements of biologically effective solar radiation using erythema weighted
708 broadband meters, *Photochem. Photobiol. Sci.*, 23, 479–492, <https://doi.org/10.1007/s43630-023-00532-z>, 2024a.

709 Czerwińska, A., and Krzyścin, J.: Modeling of Biologically Effective Daily Radiant Exposures over Europe from
710 Space Using SEVIRI Measurements and MERRA-2 Reanalysis, *Remote Sens.*, 16 (20), 3797,
711 <https://doi.org/10.3390/rs16203797>, 2024b.

712 Dave, J.V. and Halpern, P.: Effect of changes in ozone amount on the ultraviolet radiation received at sea level of
713 a model atmosphere, *Atmos. Environ.* 10(7), 547-555, [https://doi.org/10.1016/0004-6981\(76\)90181-5](https://doi.org/10.1016/0004-6981(76)90181-5), 1976.

714 den Outer, P. N., Slaper, H., Kaurola, J., Lindfors, A., Kazantzidis, A., Bais, A. F., Feister, U., Junk, J., Janouch,
715 M., and Josefsson, W.: Reconstructing of erythema ultraviolet radiation levels in Europe for the past 4 decades,
716 *J. Geophys. Res.*, 115, D10102, <https://doi.org/10.1029/2009JD012827>, 2010.

717 Downham, T. F. 2nd: The shadow rule: a simple method for sun protection, *South Med J.*, 91 (7), 619–623, 1998.

718 ERA5: ERA5 hourly data on single levels from 1940 to present,
719 <https://cds.climate.copernicus.eu/datasets/reanalysis-era5-single-levels?tab=overview>, last access 15 April 2025.

720 ESRL: The NOAA Earth System Research Laboratories,
721 <https://www.esrl.noaa.gov/gmd/grad/neubrew/SatO3DataTimeSeries.jsp>, last access 6 May 2026.

722 Farman, J., Gardiner, B., and Shanklin, J.: Large losses of total ozone in Antarctica reveal seasonal ClO_x/NO_x
723 interaction, *Nature*, 315, 207–210, <https://doi.org/10.1038/315207a0>, 1985.

724 Giovanni: The Bridge Between Data and Science v 4.40: <https://giovanni.gsfc.nasa.gov/giovanni/>, last access 15
725 April 2025.

726 GMAO: Global Modeling and Assimilation Office, MERRA-2 tavg1_2d_rad_Nx: 2d,1-Hourly, Time-Averaged,
727 Single-Level, Assimilation, Radiation Diagnostics V5.12.4, Greenbelt, MD, USA, Goddard Earth Sciences Data
728 and Information Services Center (GES DISC), <https://doi.org/10.5067/Q9QMY5PBNV1T>, last access 15 April
729 2025.

730 Gröbner, J., Hülsen, G., Vuilleumier, L., Blumthaler, M., Vilaplana, J. M., Walker, D., and Gill, J. E.: Report of
731 the PMOD/WRC-COST Calibration and Intercomparison of Erythral Radiometers. Physical Meteorological
732 Observatory Davos World Radiation Center (PMOD-WRC) Pub., 119 pp, Brussels, Belgium, 2009.

733 Hülsen, G., and Gröbner, J.: Characterization and calibration of ultraviolet broadband radiometers measuring
734 erythemally weighted irradiance, *Appl. Opt.*, 46 (23), 5877–5886, <https://doi.org/10.1364/AO.46.005877>, 2007.

735 Koepke, P., De Backer, H., Bais, A., Curylo, A., Eerme, K., Feister, U., Johnsen, B., Junk, J., Kazantzidis, A.,
736 Krzyścin, J., Lindfors, A., Olseth, J. A., den Outer, P., Pribulova, A., Schmalwieser, A. W., Slaper, H., Staiger,
737 H., Verdebout, J., Vuilleumier, L., and Weihs, P.: Modelling solar UV radiation in the past: Comparison of
738 algorithms and input data, *Proc. SPIE*, 6362, Remote Sensing of Clouds and the Atmosphere XI, 636215,
739 <https://doi.org/10.1117/12.687682>, 2006.

740 Koskela T., Taalas, P., and Leszczynski, K.: Correction method for Robertson Berger type ultraviolet radiometer
741 data, *Proc. 8th Conference on Atmospheric Radiation*, Nashville, Tennessee, USA, 161–163, 1994.

742 Krzyścin, J. W.: Biologically effective solar radiation (daily radiant exposure and irradiance at noon) at Belsk from
743 1 January 1976 to 31 December 2023 based on homogenised measurements with broadband radiometers, IG PAS
744 [dataset],
745 https://doi.org/10.25171/InstGeoph_PAS_IGData_Biologically_Effective_Solar_Radiation_Belsk_1976_2023,
746 2024.

747 Krzyścin, J. W., and Puchalski, S.: Aerosol impact on the surface UV radiation from the ground-based
748 measurements taken at Belsk, Poland, 1980–1996, *J. Geophys. Res.*, 103 (D13), 16175–16181, 1998.

749 Krzyścin, J. W., Sobolewski, P. S., Jarosławski, J., Podgórski, J., and Rajewska-Więch, B.: Erythral UV
750 observations at Belsk, Poland, in the period 1976–2008: Data homogenization, climatology, and trends, *Acta*
751 *Geophys.*, 59, 155–182, <https://doi.org/10.2478/s11600-010-0036-3>, 2011.

752 Krzyścin, J. W., Jarosławski, J., Rajewska-Więch, B., Sobolewski, P. S., Narbutt, J., Lesiak, A., and Pawlaczyk,
753 M.: Effectiveness of heliotherapy for psoriasis clearance in low and mid-latitudinal regions: A theoretical
754 approach, *J. Photochem. Photobiol. B Biol.*, 115, 35–41, <https://doi.org/10.1016/j.jphotobiol.2012.06.008>, 2012.

755 Krzyścin, J. W., Sobolewski, P., Czerwińska, A., Rajewska-Więch, B., Jarosławski, J.: Biologically weighted
756 daily radiant exposure for erythema appearance, previtamin D₃ synthesis and clearing of psoriatic lesions from
757 erythema biometers at Belsk, Poland, for the period 1976–2023, PANGAEA
758 [dataset], <https://doi.org/10.1594/PANGAEA.972139>, 2024.

759 Leszczynski, K., Jokela, K., Ylianttila, L., Visuri, R., Blumthaler, M.: Erythemally Weighted Radiometers in Solar
760 UV Monitoring: Results from the WMO/STUK Intercomparison, *Photochem. Photobiol.*, 67 (2), 212–221,
761 <https://doi.org/10.1111/j.1751-1097.1998.tb05189.x>, 1998.

762 Madronich, S.: UV radiation in the natural and perturbed atmosphere, in: UV-B Radiation and Ozone Depletion.
763 Effects on Humans, Animals, Plants, Microorganisms, and Materials, edited by: Tevini, M., Lewis, Boca Raton,
764 Ann Arbor, London, UK, Tokyo, Japan, 17-69, 1993

765 Molina, M. J., and Rowland, F. S.: Stratospheric sink for chlorofluoromethanes: chlorine atom-catalyzed
766 destruction of ozone, *Nature*, 249, 810–812, <https://doi.org/10.1038/249810a0>, 1974.

767 NDACC, Network for the Detection of Atmospheric Composition Change, [https://www-](https://www-air.larc.nasa.gov/missions/ndacc/)
768 [air.larc.nasa.gov/missions/ndacc/](https://www-air.larc.nasa.gov/missions/ndacc/), last access: 15 April 2025.

769 Neale, R. E., Lucas, R. M., Byrne, S. N., Hollestein, L., Rhodes, L. E., Yazar, S., Young, A. R., Berwick, M.,
770 Ireland, R. A., and Olsen, C. M.: The effects of exposure to solar radiation on human health, *Photochem. Photobiol.*
771 *Sci.*, 22, 1011–1047, <https://doi.org/10.1007/s43630-023-00375-8>, 2023.

772 Posyniak, M., Szkop, A., Pietruczuk, A., Podgórski J., and Krzyścin, J.: The long-term (1964-2014) variability of
773 aerosol optical thickness and its impact on solar irradiance based on the data taken at Belsk, Poland, *Acta Geophys.*,
774 64, 1858–1874, <https://doi.org/10.1515/acgeo-2016-0026>, 2016.

775 Puchalski, S.: Preliminary results of the comparison of Robertson-Berger meter with the UV-Biometer MOD
776 501A, version 3, produced by Solar Light Co., *Publs. Inst. Geophys. Pol. Acad. Sc. D-42(269)*, 113–115, 1995.

777 Rieder, H. E., Holawe, F., Simic, S., Blumthaler, M., Krzyścin, J. W., Wagner, J. E., Schmalwieser, A. W., and
778 Weihs, P.: Reconstruction of erythema UV-doses for two stations in Austria: a comparison between alpine and
779 urban regions, *Atmos. Chem. Phys.*, 8, 6309–6323, <https://doi.org/10.5194/acp-8-6309-2008>, 2008.

780 Schmalwieser, A. W., Eschenbacher, S., and Schreder, J.: UV-Biometer - The usage of erythema weighted
781 broadband meters for other biological effects, *J. Photochem. Photobiol. B Biol.*, 230, 112442,
782 <https://doi.org/10.1016/j.jphotobiol.2022.112442>, 2022.

783 Scotto, J., Cotton, G., Urbach, F., Berger, D., and Fears, T.: Biologically effective ultraviolet radiation: surface
784 measurements in the United States, 1974 to 1985, *Science*, 239 (4841), 762–764,
785 <https://doi.org/10.1126/SCIENCE.3340857>, 1988.

786 Słomka, J., and Słomka, K.: Comparison of Robertson-Berger ultraviolet meter counts with the UVB and Uver
787 radiation inflow determined from Dave-Halpern’s model, *Publs. Inst. Geophys. Pol. Acad. Sc.*, D-22 (189), 133–
788 143, 1985.

789 Słomka, J., and Słomka, K.: Biologically active solar UV radiation at Belsk in the years 1976-1992, *Publs. Inst.*
790 *Geophys. Pol. Acad. Sc.*, D-40 (263), 71–81, 1993.

791 TUV: Tropospheric Ultraviolet and Visible (TUV) Radiation Model:
792 <https://www2.acom.ucar.edu/modeling/tropospheric-ultraviolet-and-visible-tuv-radiation-model>, last access 15
793 April 2025.

794 Volpert, E.V., and Chubarova, N.E.: Long-term changes in solar radiation in Northern Eurasia during the warm
795 season according to measurements and reconstruction model. *Russ. Meteorol. Hydro+*, 46(8), 507–518,
796 <https://doi.org/10.3103/S1068373921080021>, 2021.

797 Weatherhead, E. C., Reinsel, G. C., Tiao, G. C., Meng, X., Choi, D., Cheang, W., Keller, T., DeLuisi, J., Wuebbles,
798 D. J., Kerr, J. B., Miller, A. J., Oltmans, S. J., and Frederick, J. E.: Factors affecting the detection of trends:
799 Statistical considerations and applications to environmental data, *J. Geophys. Res.*, 103 (D14), 17149–17161,
800 <https://doi.org/10.1029/98JD00995>, 1998.

801 WMO: World Meteorological Organization, UNEP, Report of the Meeting of Experts on UV-B Monitoring and
802 Research, GORMP-No. 03, WMO, Geneva, Switzerland, 1977.

803 WOUDC: World Ozone and Ultraviolet Radiation Data Centre, <https://woudc.org/data.php>, last access 15 April
804 2025.

805

806

807